Journal of Catalysis 284 (2011) 9–22

Contents lists available at SciVerse ScienceDirect

Journal of Catalysis

journal homepage: www.elsevier.com/locate/jcat

Modified alumina as catalyst support for cobalt in the Fischer–Tropsch synthesis

Bjørn Christian Enger [a], Åse-Lill Fossan [a,1], Øyvind Borg [a,b], Erling Rytter [a,b], Anders Holmen [a,*]

[a] Department of Chemical Engineering, Norwegian University of Science and Technology (NTNU), N-7491 Trondheim, Norway
[b] Statoil Research Centre, Postuttak, N-7005 Trondheim, Norway

ARTICLE INFO

Article history:
Received 16 February 2011
Revised 12 August 2011
Accepted 13 August 2011
Available online 25 September 2011

Keywords:
Fischer–Tropsch synthesis
Modified alumina
Water
Co
Zn
Mg
Ni
Re

ABSTRACT

The effect of different modifications (Zn, Mg, Ni, Re) has been studied for alumina-supported 12 wt% Co-catalysts in the Fischer–Tropsch synthesis (FTS) using a fixed-bed reactor at 483 K, 20 bar, and $H_2/CO = 2$. Different parameters including calcination temperature, loading, impregnation sequence, and water partial pressure during FTS have been studied. When compared to low surface area α-Al_2O_3, mechanical strength was substantially improved for Ni- and Mg-modified aluminas calcined at very high temperatures (>1400 K), thus making them more suitable for slurry or fluidized-bed operation. However, Mg was found to have a loading-dependent negative effect on both activity and selectivity. The wt% effect was stronger when co-impregnated with Co–Re and calcined at 773 K, than when impregnated on the support and calcined at a high temperature (1173 K) prior to impregnation with Co–Re. Co-impregnating Co–Re with Zn also had a strong loading-dependent negative effect on activity and selectivity, while impregnating Zn on the support and calcining at a high temperature (1173 K) prior to impregnation with Co–Re had no negative effect on the overall C_{5+} yield. The negative effects of Mg and Zn could not be explained by dispersion or particle size effects and were likely related to a chemical/site effect similar to that of alkalies reported on in the literature. The effect of water for the Ni-modified support was in accordance with the literature, improving reaction rates and C_{5+} selectivity, while inhibiting olefin hydrogenation, as demonstrated by the propene/propane ratio. The catalysts were characterized with H_2 chemisorption, N_2 sorption, mercury intrusion, X-ray diffraction, temperature-programmed reduction, and O_2 titration.

1. Introduction

The purpose of modern Fischer–Tropsch synthesis (FTS) is the value-added conversion of natural gas or gasified carbon resources to high-quality waxes and diesel fuel. For natural gas–based processes, delivering H_2/CO close to 2.0, cobalt is the preferred catalyst, with high selectivity to long-chain hydrocarbons (waxes). Iron catalysts are preferred for direct conversion to mid-range (diesel) products based on coal as a feedstock. Water–gas-shift activity is higher in the presence of iron, and it is, therefore, possible to operate at lower H_2/CO feed ratios. Iron catalysts are also more tolerant to feed contamination from alkali and alkaline earth metals than cobalt; in fact, potassium is beneficial for improving the activity and selectivity of iron catalysts [1]. For cobalt-based catalysts, the selectivity to long-chain hydrocarbons (C_{5+}) depends on a number of different factors including the support material, Co dispersion, and reaction conditions (e.g., gas velocity, residence time, partial pressures, and temperature).

For industrial applications using, e.g., slurry or fluidized-bed reactors, mechanical strength is a parameter that has to be optimized. The attrition of a catalyst, which is a measure of the degree of abrasion and fracturing of catalyst pellets during operation and catalyst handling, can be influenced by modifying the support. If the support is too weak, the breakdown of these solid particles will produce substantial amounts of particle fines (micron and sub-micron powders). This fine powder affects not only fluidization properties (e.g., foaming) but may also plug solid–liquid separation filters and contaminate the wax product.

The full commercial potential for any catalytic system can only be properly addressed after optimizing catalyst activity and selectivity. In the Fischer–Tropsch synthesis, the selectivity to long-chain hydrocarbons and the rate of reaction determine the overall productivity or yield. Several factors are important for optimizing productivity, such as: the site-time yield on the catalytic surface, possible differences in site activity and/or selectivity, local temperature gradients (hot spots), local concentrations of reactants, and products as well as possible transport limitations. Some of these factors can be accounted for by obtaining kinetically relevant data in the absence of transport limitations and hot spots. This typically requires careful control of the temperature, and in order to avoid intra-particle diffusion limitations, the catalyst pellet

* Corresponding author. Fax: +47 73 59 50 47.
E-mail address: holmen@chemeng.ntnu.no (A. Holmen).
[1] Present address: Esso Norge, Slagen, Boks 2001, N-3103 Tønsberg, Norway.

0021-9517/$ - see front matter © 2011 Elsevier Inc. All rights reserved.
doi:10.1016/j.jcat.2011.08.008

diameter must be sufficiently small. Then, possible differences in site activity or selectivity can be addressed as a function of catalyst composition.

The Fischer–Tropsch reactions proceed in a manner which for decades was believed to be *structure insensitive*. However, recent research has demonstrated that structural effects become evident for particles smaller than about 5–7 nm [2–4]. For larger particles, the calculated average turnover frequency (TOF) and, thus, also the averaged site-time yield (STY) is still largely unaffected by the support material [5,6], the cobalt loading and dispersion [6,7]. The same has been observed with respect to the surface orientation of cobalt single crystals and for films [8–11]. Steady-state isotopic transient kinetic analysis (SSITKA) of CO hydrogenation on a large number of different cobalt catalysts has also concluded with an apparent structure insensitivity [12–14], again provided that the Co-particles are larger than about 5–7 nm. It has been claimed that the reason for the apparent variations in calculated TOF's or STY's is differences in surface coverage of active intermediates. The apparent structure insensitivity of FTS was even earlier argued to be caused by an almost complete surface coverage of reactive intermediates derived from CO, which is reflected by the negative reaction order of CO [15,16]. Deviations from this apparent structure insensitivity, such as the observations by Fu and Bartholomew [17], are usually explained by an incomplete reduction of Co oxides. For Co supported on carbon nanofibers, it was recently shown that for Co-particles smaller than 5–7 nm, the turnover frequency strongly depended on the Co particle size [2–4]. It was concluded that the reduced turnover frequency of the smaller particles (<6 nm) was caused by both blocking of edge/corner sites and a lower intrinsic activity at the small terraces. The term structure insensitive is, thus, inadequate, in particular, when looking into reaction mechanisms, as it only expresses an apparent approximation based on the averaged experimental data under certain conditions (e.g., large particles, well-covered surface).

Because it has been recognized that the degree of reduction is such an important parameter, the dispersion and reducibility of cobalt oxide species have been much investigated on different supports [18–22]. The effects of reduction promoters such as Pt, Pd, Ru, and Re have also been studied extensively [23–26]. Several excellent reviews have addressed the topics of kinetics, selectivity, and reaction mechanisms [16,27–29]. Different explanations have been proposed for variations in selectivity, but the overall model described by Iglesia et al. [27], Fig. 1, still provides one of the most suitable illustrations for discussing variations in selectivity with respect to intrinsic rate parameters.

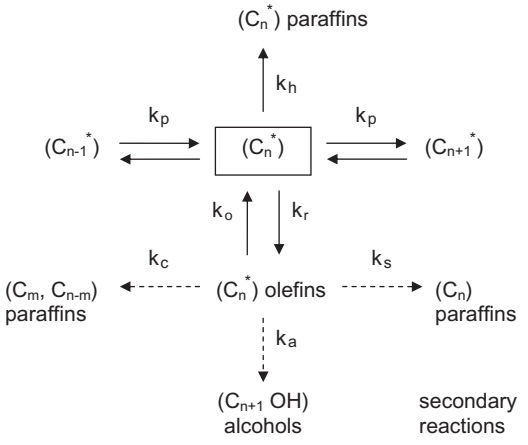

Fig. 1. Illustration of chain growth and termination parameters in the Fischer–Tropsch synthesis by Iglesia et al. [27]. Rate constants (k) are for; hydrogenation (k_h), chain propagation (k_p), hydrogen abstraction (k_r), olefin re-adsorption (k_o), catalytic cracking (k_c), secondary hydrogenation of olefins (k_s), and hydroxylation to alcohols (k_a).

Large differences with respect to selectivity have been observed depending on support material [18–22,30–33], yet most of the discussions have revolved around the same explanations. The pore size effect [20,34–37] and the pore size versus particle size effect [20,38] are both structurally related effects, which is a theme that extends to include also the effect of pore tortuosity on the effective diffusivity of reactants and products [39,40]. There is no doubt that C_{5+} selectivity appears to increase with increasing Co particle sizes up to a certain level [21,41], an observation which applies to most supports. However, it has typically not been possible to isolate this effect from the effect of pore structure without also changing other parameters such as, e.g., surface acidity or degree of reduction. By studying carbon nanofiber-supported catalysts, it was recently shown that C_{2+} selectivity during CO hydrogenation was independent of Co particle size for Co particles >6 nm [2]. For particles <6 nm, the selectivity to methane increased with decreasing particle size. A higher surface coverage of hydrogen was measured for particles <6 nm, thus increasing the probability for hydrogenation reactions. Bezemer et al. [4] reported substantially increased octane/octene ratios for particles <5 nm during Fischer–Tropsch synthesis, also indicating increased hydrogenation activity.

The second general theme for explaining differences in selectivity is related to the active site itself. This includes effects from site-blocking or electronic effects from chemical site poisoning by (un)reactive intermediates or other elements (e.g., Na, K). Electronic modifications of the active site affects the binding energy, and thus the activation energy barriers of elementary surface reactions, from which the initial product composition is largely determined, given the local concentrations of reactants and products. Referring to Fig. 1, site poisoning or site blocking can explain differences in selectivity by decreasing different intrinsic rates of chain propagation, chain termination, or re-adsorption of reactive intermediates. Because of differences in binding energies, different sites will have different coverage-dependent intrinsic rates, thus affecting not only activity but also the intrinsic selectivity. Differences in coverage-dependent binding energies will be mirrored in the measured differences in the surface residence time and concentration of reactants, products and intermediates. These species compete for the different sites (i.e., sites with different coordination numbers), and their coverage-dependent binding energy to a specific site will greatly influence the outcome of this competition. Binding energies may also depend on the size of the metal particle, and an explanation for the effect of the Fermi level on the binding energy of CO to small Co (<7 nm) particles was recently included in a review of biomass to liquids by van Steen and Claeys [26]. Whatever is the proper combination of effects, there is no doubt that the site itself and the presence of other elements on the surface is a governing theme with respect to understanding both selectivity and activity.

The purpose of this work has been to investigate the effect of support and catalyst modifications, including Ni, Mg, Zn, and Re. The reason for studying low surface area alumina was that very high C_{5+} selectivity was previously reported by Schanke et al. [42]. However, it is known that low surface area alpha-alumina does not have proper mechanical strength for use as a slurry reactor catalyst [27]. Thus, the reason for adding Ni or Mg was to stabilize and strengthen the alumina by forming spinel structures ($NiAl_2O_4$ or $MgAl_2O_4$). Such modifications may not only affect attrition properties, catalyst dispersion, and reducibility but can also change both catalytic activity and selectivity. Only a few studies have previously been reported investigating Mg [33,43] and Zn [44–49] as modifications to Co in FTS. The results on Mg were not conclusive as Zhang et al. [33] reported negative effects from Mg on both activity and C_{5+} selectivity, while Guerrero-Ruiz reported positive effects [43]. Madikizela and Coville [44–48] studied Zn as a promoter for Co/TiO_2 catalysts,

Table 1
Catalyst properties[a] and steady-state results from fixed-bed testing of activity and selectivity in the Fischer–Tropsch synthesis at 483 K, 20 bar and $H_2/CO = 2$. The four sections of the table: (1) 1–2; standard temperature calcined (773 K) Co(Re) on γ-Al_2O_3 (178 m^2/g), (2) 3–8; catalysts on high-temperature calcined (>1400 K) alumina and modified aluminas, (3) 9–14; catalysts on intermediately calcined (1173 K) modified aluminas, and (4) 15–21; standard-temperature calcined (773 K) co-impregnated modified catalysts.

#	Support	Co wt%	Re wt%	Zn wt%	Mg wt%	Ni wt%	BET (m^2/g)	PV (ml/g)	DOR (%)	H:Co (%)	Co-d_p (nm)	XRD-d_p (nm)	H_2-v_{ads} (Nml/g)	[b]Run #	[c]rCO (mol/g h)	[c]Co t.y. (s^{-1}) [e]	[c]$STY_{H\text{-}sat}$ (s^{-1})	[d]SCH_4 (%)	[d]SC_{5+} (%)	[d]$STY_{H\text{-}sat}$ (s^{-1})
1	γ-Al_2O_3	12	–	–	–	–	154	0.57	57	6.7	14	14	1.54		0.0297	44	0.07	9.4	80.0	0.06
2	γ-Al_2O_3	12	0.5	–	–	–	155	0.57	65	9.4	10	13	2.18		0.0370	55	0.06	8.5	83.2	0.06
3	α-Al_2O_3	12	–	–	–	–	8.5	0.25	65	2.7	35	32	0.63		0.0132	19	0.07	8.2	83.2	0.08
4	α-Al_2O_3	12	0.5	–	–	–	13.5	0.25	71	3.7	26	29	0.85		0.0228	34	0.09	7.4	86.7	0.10
5	$NiAl_2O_4$-α-Al_2O_3	12	–	–	–	5	13.3	0.20	66	3.8	26	n.a.	0.87	a	0.0164	24	0.06	9.5	79.7	0.08
"														b	0.0169	25	0.07	8.9	80.8	0.11
6	$NiAl_2O_4$-α-Al_2O_3	12	0.5	–	–	5	18.0	0.20	70	4.7	21	n.a.	1.08	a	0.0246	36	0.08	8.3	83.9	0.07
"														b	0.0229	34	0.07	8.8	82.9	0.08
7	$MgAl_2O_4$-α-Al_2O_3	12	–	–	10	–	18.3	0.12	60	5.3	18	n.a.	1.23		0.0127	19	0.04	8.9	80.9	0.04
8	$MgAl_2O_4$-α-Al_2O_3	12	0.5	–	10	–	22.8	0.12	67	6.2	16	n.a.	1.42		0.0180	27	0.04	8.0	83.3	0.04
9	1%Mg-γ-Al_2O_3	12	0.5	–	1	–	105	0.53	n.a.	9.7	10	10	2.24		0.0271	37	0.04	8.1	82.3	0.04
10	5%Mg-γ-Al_2O_3	12	0.5	–	5	–	74	0.37	n.a.	10.0	10	10	2.31	a	0.0267	36	0.04	8.2	81.8	0.04
"														b	0.0290	40	0.04	9.2	80.6	0.04
11	10%Mg-γ-Al_2O_3	12	0.5	–	10	–	65	0.34	n.a.	9.3	10	10	2.15		0.0154	21	0.02	9.4	76.6	0.02
12	1%Zn-γ-Al_2O_3	12	0.5	1	–	–	103	0.53	n.a.	9.5	10	10	2.20		0.0399	54	0.06	8.7	82.1	0.06
13	5%Zn-γ-Al_2O_3	12	0.5	5	–	–	95	0.47	n.a.	9.3	10	10	2.15		0.0437	60	0.06	8.8	82.5	0.06
14	10%Zn-γ-Al_2O_3	12	0.5	10	–	–	87	0.41	n.a.	10.2	9	10	2.36		0.0374	51	0.05	9.0	82.4	0.05
15	γ-Al_2O_3	12	0.5	–	0.01	0.01	150	0.56	n.a.	9.0	11	11	2.08	a	0.0393	54	0.06	9.1	81.8	0.06
"														b	0.0372	51	0.06	9.1	82.0	0.06
16	γ-Al_2O_3	12	0.5	–	0.1	0.1	148	0.56	n.a.	8.8	11	11	2.04		0.0289	39	0.05	9.2	80.7	0.04
17	γ-Al_2O_3	12	0.5	–	1	1	146	0.53	n.a.	9.2	10	10	2.13		0.0155	21	0.02	11.0	72.4	0.02
18	γ-Al_2O_3	12	0.5	1	–	–	149	0.54	n.a.	7.5	13	13	1.73		0.0312	43	0.06	10.2	79.7	0.06
19	γ-Al_2O_3	12	0.5	2	–	–	148	0.53	n.a.	5.3	18	18	1.23		0.0195	27	0.05	10.3	76.8	0.07
20	γ-Al_2O_3	12	0.5	5	–	–	144	0.50	n.a.	3.8	25	25	0.88		0.0025	3	0.01	n.a.	n.a.	n.a.
21	γ-Al_2O_3	12	0.5	5	–	–	140	0.51	n.a.	4.5	21	21	1.04		0.0071	10	0.02	n.a.	n.a.	n.a.

[a] wt%: all loadings are nominal values given as wt% metal/Al_2O_3; BET: surface area (Brunauer–Emmett–Teller); PV: pore volume; DOR: degree of reduction from O_2 titration; H:Co is a measure of catalyst dispersion assuming 100% DOR and H:Co adsorption stoichiometry of 1:1; Co-d_p is the particle size calculated using H:Co as a measure of catalyst dispersion; XRD-d_p is the particle size calculated from the Scherrer thickness of Co_3O_4. n.a. (not available).

[b] Run numbers *a*/*b* are repeated runs for the same catalyst, included to illustrate the small degree of uncertainty for the data set. n.a.: not available.

[c] Initial activity data, including cobalt-time yields (Co t.y.) mostly obtained after 8 h on stream, see also [c].

[d] Activity and selectivity data obtained after adjusting the gas velocity to obtain about 50% CO conversion. When necessary, data have been extrapolated from the range 45–55% CO conversion to exactly 50%. Co t.y. (cobalt-time yield); $STY_{H\text{-}sat}$ (site-time yield from *ex situ* H-saturation coverage, i.e., total H_2 chemisorpion); X_{CO} (conversion of CO); SCH_4 (selectivity to CH_4); SC_{5+} (selectivity to C_{5+}); n.a. (not available). For catalyst No. 19, CO conversion increased through the entire initial 24-h period. For catalysts No. 20, the initial CO conversion was <2% after 24 h, and for catalyst No. 21, it reached at maximum of 5.6% CO conversion after 74 h, neither could therefore be adjusted to 50% CO conversion.

[e] Actually (mol CO/mol cobalt · s).

including the effects of impregnation sequence [44], sol–gel synthesis [45], sulfur tolerance [46], Zn loading [47], and Co and Zn precursors [48]. For these catalysts, a positive effect on both conversion and selectivity to C_{5+} was observed for 5 wt% Zn, when this was added to TiO_2 before impregnating with Co. The positive effect on activity was observed for all; however, with 10 wt% Zn or when Co and Zn were co-impregnated, or when Zn was impregnated after Co, the product composition was shifted toward lighter hydrocarbons. With 10 wt% Zn, about 40% of the product was methane. Ni is one of the metals that Fischer and Tropsch found to be active for CO hydrogenation; however, it was soon discovered that a catalyst, where Ni was the active phase, yielded a light product range dominated by methanation. A summary of studies on Ni in the Fischer–Tropsch synthesis is far beyond the scope of this introduction. Many studies were carried out on Nickel–Thoria–Kieselguhr during the 1940–1950s. Interestingly, recent work by Rytter et al. [50] indicates that Ni may substitute for Re as a reduction and activity promoter for Co catalysts. Another interesting property of Ni is that its divalent metal ion enables spinel ($NiAl_2O_4$) formation, a material with a mechanical strength superior to alumina, making it more suitable for slurry or fluidized-bed operation. For FTS, this property was first explored by Rytter et al. [51]. This material may also have interesting properties as a catalyst precursor [52].

2. Experimental

2.1. Catalyst preparation

Cobalt and cobalt–rhenium catalysts were prepared by one-step *incipient wetness* co-impregnation of different (modified) supports with aqueous solutions of $Co(NO_3)_2{\cdot}6H_2O$ (Acros organics, >99%) and $HReO_4$ (Alfa Aesar, Johnson Matthey GmbH, 75–80% aq. soln.). The catalysts (20 g) were dried in air at 383 K for 3 h before calcination in flowing air (200 ml/min), increasing the temperature at 2.5 K/min from ambient to 573 K and holding for 16 h. The calcined samples were then sieved, and the 53–90 μm samples were collected. Further, pretreatment was done *in situ*. Catalyst properties are summarized in Table 1, including details from characterizations with XRD, H_2 chemisorption, and N_2 sorption as well as results from fixed-bed Fischer–Tropsch activity testing.

α-Al_2O_3 support was prepared by treating γ-Al_2O_3 (Puralox SCCa-45/190) support with air at 1413 K for 10 h. The $NiAl_2O_4$-α-Al_2O_3 support was prepared by *incipient wetness* impregnation of the γ-Al_2O_3 with $Ni(NO_3)_2{\cdot}6H_2O$ (Acros organics, >99%) and then treated with air at 1433 K for 12 h. The nominal loading prior to high-temperature calcination was 5 wt% Ni/Al_2O_3. The $MgAl_2O_4$-α-Al_2O_3 support was prepared by *incipient wetness* impregnation of γ-Al_2O_3 with $Mg(NO_3)_2{\cdot}6H_2O$ (Acros organics, >99%) and then treated with air at 1413 K for 10 h. The nominal loading prior to high-temperature calcination was 10 wt% Mg/Al_2O_3. Six different Mg-γ-Al_2O_3 and Zn-γ-Al_2O_3 supports (1, 5, and 10 wt% Mg or Zn) were prepared by impregnation of a pre-calcined γ-Al_2O_3 using $Mg(NO_3)_2{\cdot}6H_2O$ (Acros organics, >99%) and $Zn(NO_3)_2{\cdot}6H_2O$ (Fluka, >99%) precursors, followed by drying at 383 K for 3 h and then treated with air at 1173 K for 16 h. The effect of Mg and Zn as support modifications was contrasted by co-impregnating Mg (0.01, 0.1 or 1 wt%) or Zn (1, 2 or 5 wt%) together with 12 wt% Co and 0.5 wt% Re on γ-Al_2O_3, using the same precursors as above. These are all nominal loadings given as wt% metal/support.

2.2. Surface area and pore volume measurements with N_2, H_2, or mercury intrusion

Isotherms from volumetric adsorption and desorption of nitrogen were measured at the boiling point of liquid nitrogen using a standard commercial equipment (Micromeritics Tristar 3000). The sample (0.5 g) was placed in the quartz container, vacuum dried at 573 K for 1 h, and cooled to room temperature before the measurements. The surface area and pore volume were calculated using the BET [53] and the BJH [54] methods, respectively. The BJH method was applied assuming a slit pore shape followed by stepping off the desorbed volume by using the Kelvin equation and a film thickness equation.

Isotherms from volumetric chemisorption of hydrogen were measured at 313 K or 333 K in a standard glass apparatus (Micromeritics ASAP 2010) capable of achieving a vacuum of 10^{-3} Pa or better. The sample (0.2–0.4 mg) was placed in a U-tube quartz reactor, dried and evacuated at 313 K (1 h), and reduced in flowing hydrogen by ramping at 1 K/min from ambient to 623 K and holding for 10 h. The sample was evacuated for 1 h at 623 K and cooled to 313 K (or 333 K) before the chemisorption isotherms were obtained. It was assumed that Re did not contribute to the amount of hydrogen chemisorbed [55]. The obtained H:Co ratio is only a measure of catalyst dispersion if: (a) it is assumed that the adsorption stoichiometry is H:Co = 1 [56] and (b) the degree of reduction is close to 100%. Increasing the chemisorption temperature from 313 to 333 K has been shown to increase the H:Co ratio by a factor of 1.07–1.09 for similar Co/Re catalysts [57]. This effect has been accounted for by increasing the H:Co ratio obtained at 313 K by a factor of 1.08. The hydrogen to Co ratio (H:Co), which is a measure of the surface area of metallic cobalt when the loading of Co is the same for all catalysts, was calculated using Eq. (1):

$$\mathrm{H:Co} = C_t \frac{M_{\mathrm{Co}}}{x_{\mathrm{Co}}} \tag{1}$$

$C_t = V_{\mathrm{ads}}/22{,}711$ is the total concentration of sites (mol/g), where V_{ads} was obtained from an extrapolation of the linear part of the isotherm to zero pressure, 22,711 N cm^3/mol is the ideal gas volume at 1 bar and 273 K. x_{Co} is the mol fraction of cobalt, and M_{Co} is the molar mass of cobalt. No chemisorption of H_2 was found on the supports.

Pore volumes for low surface area catalysts were obtained on a Carlo Erba Macropores Unit 120, Carlo Erba Porosimeter 2000, and Carlo Erba Multisampler 190. The pore diameters were calculated using a force balance Eq. (2) for a cylindrical pore assuming a surface tension of 480 mN/m and a wetting angle of 141.3° for mercury.

$$d = \frac{15{,}000}{p(bar)}(nm) \tag{2}$$

2.3. Measurements of catalyst reducibility

Temperature-programmed reduction (TPR) was carried out in a U-shaped tubular quartz reactor heated by an electrical furnace [58]. The sample (0.2 g) was exposed to a reducing gas mixture consisting of 7% H_2 in argon, while the temperature was increased from ambient to 1203 K at 10 K/min. A cold trap containing a mixture of 2-propanol and dry ice was used to eliminate water and other condensable products from the product gas mixtures. The consumption of hydrogen was measured by analyzing the effluent gas with a thermal conductivity detector (TCD).

The degree of reduction (DOR) was obtained by O_2 titration using the same apparatus as for TPR measurements. The catalyst sample (0.10 g) was reduced in a U-tube quartz reactor using flowing hydrogen for 16 h. The hydrogen flow rate was 45 ml/min, and the helium carrier gas pressure was adjusted to 1.0 ± 0.15 bar. The sample was heated from room temperature to 623 K at 1 K/min and was then kept at 623 K for 10 h. Pre-treatment was turned off, and the sample was heated at 2 K/min up to 673 K in pure helium flow. The sample was kept at 673 K for 1 h before calibrated oxygen pulses were

passed through the system. The oxygen pulses were added to the continuous flow of helium until no further consumption of oxygen was detected by the thermal conductivity detector downstream of the reactor. The degree of reduction was calculated assuming stoichiometric re-oxidation of metallic cobalt to Co_3O_4.

2.4. Phase properties and mechanical strength

X-ray diffraction spectra were obtained using a Siemens D5005 X-ray diffractometer with monochromatic Cu Kα radiation, $\lambda = 0.1542$ nm [59], operating at 40 kV and 50 mA. The results were used to verify the presence of the three-dimensional spinel structures $NiAl_2O_4$ and $MgAl_2O_4$ and to estimate the diameter of the cobalt particles using the Scherrer [60] thickness (t) of Co_3O_4, Eq. (3).

$$t = \frac{K\lambda}{\Delta(2\theta)\cos(\theta)} = 0.75 \cdot d_{Co_3O_4} = d_{Co} \quad (3)$$

The K factor was set to 0.89 [61], and instrumental line broadening was accounted for in $\Delta(2\theta)$, as determined from XRD of LaB_6 (Lanthanaum Hexaboride). The diffraction lines associated with $NiAl_2O_4$ and $MgAl_2O_4$ overlap those from Co_3O_4 making particle size determination very uncertain for catalysts supported on $NiAl_2O_4$–α-Al_2O_3 and $MgAl_2O_4$–α-Al_2O_3. Those estimates were, therefore, omitted in Table 1.

A modified ASTM-type equipment was used for attrition measurements [62]. The custom-built equipment consists of a moisture and a separation chamber. Initially, 50 g (>40 μm) was loaded into the separation chamber. Pressurized air was then passed through the moisture chamber and then through sieve trays to the separation chamber. In this way, the pre-loaded sample was exposed to sonic air flow, resulting in grinding of the particles. Particles larger than 40 μm fell down, whereas the smaller particles entered a soxhlet filter in the top of the separation chamber. The amount of fines was measured every hour for 5 h. The attrition value reported was calculated using:

$$\text{Attrition} = \text{cumulative amount of fines after 5 h} / \text{total amount of sample (50 g)}.$$

2.5. Measurements of fixed-bed activity and selectivity

Fischer–Tropsch synthesis was carried out in a unit with two parallel fixed-bed reactors (stainless steel, 10 mm inner diameter). The samples (1–2 g, 53–90 μm) were diluted with inert silicon carbide particles (3–4 g, 75–150 μm) in order to improve the temperature distribution along the catalyst beds.

The samples were reduced *in situ* by passing through hydrogen (250 N ml/min) at 623 K and 1 bar. After 16 h, the reactor was cooled to 443 K and flushed 1 h with helium (150 N ml/min). The system was then pressurized to 20 bar using 50% hydrogen in helium (250 N ml/min) before synthesis gas was introduced to the reactors ($H_2/CO = 2.0$, 3% N_2 as internal standard, 250 N ml/min). After 1 h, the reactor system was heated to 483 K at 1 K/min.

Wax and liquid products were collected in a heated trap (about 363 K), and light liquid products were removed in a cold trap (298 K). An on-line gas chromatograph (HP5090A) equipped with thermal conductivity detector (TCD) and flame ionization detector (FID) was used to analyze the effluent product stream. The equipment has been described and illustrated in more detail by Hilmen et al. [63].

After about 24 h on stream at initial conditions, the flow of feed gas was reduced in order to adjust the CO conversion to about 50%. The flow rate of synthesis gas was kept constant throughout subsequent periods (if any). Steady-state results for all catalysts are detailed in Table 1.

For catalysts 5 and 6 in Table 1, after about 25 h at 50% CO conversion, helium was added to the feed gas in order to change the partial pressures of hydrogen, CO and H_2O. Helium was then replaced by de-ionized water, which was fed from a water tank pressurized to 20 bar to a vaporizer kept at 573 K. The following co-feeds were investigated as a sequence, each period lasting about 25 h: 5 bar He, 4 bar water, 6,9 bar water, and 10 bar He. Finally, to check for deactivation caused by these changes in conditions, the catalysts were exposed to the same feed as prior to adding He or water.

The activity is reported as three parameters: the rate of CO conversion, cobalt-time yield (mol CO/mol(Co) s), and site-time yield $STY_{H\text{-}sat}$ (s^{-1}). $STY_{H\text{-}sat}$ was calculated using the total number of H sites obtained by *ex situ* hydrogen chemisorption, and thus assumes that the saturation coverage of H is a suitable measure for the number of sites. It also assumes that there is only one type of sites, i.e., it ignores any effects from the binding-site coordination number or coverage dependencies on the activation energy barriers. The C_{5+} selectivity was calculated by subtracting the amount of C_1–C_4 (including CO_2) in the effluent gas mixture from the total mass balance.

3. Results and discussion

3.1. Surface area, pore volume, and mechanical strength

The purpose of carrying out support modifications was to investigate how this affects attrition properties, catalyst reducibility, and dispersion; properties that are of the highest importance for industrial application of a Fischer–Tropsch synthesis catalyst.

Table 1 is separated into four sections. First, there is a standard Co(Re) on γ-Al_2O_3 (178 m^2/g) catalyst, which serves as a reference for our modifications. The second section contains catalysts supported on low surface area aluminas and aluminates with Ni or Mg-spinel inclusions (<25 m^2/g). These were prepared by high-temperature calcination (>1400 K). In the third section, we find catalysts prepared on modified γ-Al_2O_3 with intermediate surface areas (65–105 m^2/g). These supports were modified by Mg or Zn prior to calcination at 1173 K. At this calcination temperature, it cannot be completely excluded that phase transition to δ-Al_2O_3 may have initiated [64], even though it was not evident from our XRD data. Modifying with either Mg or Zn and calcining at 1173 K decreased the BET surface area. MgO and ZnO are substantially more difficult to reduce as compared to cobalt oxides and will likely be present as oxides and/or hydroxides during FTS. The main reason for the decreasing surface areas of supports impregnated with Mg and Zn is probably the high-temperature calcination; however, some effect attributable to MgO or ZnO cannot be excluded. For example, Zhang et al. [33] reported slightly decreasing average pore diameters when adding MgO, suggesting that MgO was coating the interior of the support, thus somewhat decreasing its surface area. A similar effect may be expected for ZnO. The fourth section of Table 1 summarizes catalysts where the modification (Zn or Mg) was added as a promoter during co-impregnation of Co and Re followed by calcination at 573 K.

As already mentioned, the poor mechanical strength of the α-Al_2O_3 support makes it unsuitable for slurry or fluidized-bed operation. Still, it shows excellent selectivity to C_{5+} products [42], which makes it interesting. Increasing the mechanical strength by spinel formation is not new, and reports and patents on preparation and different applications of aluminate spinels have appeared since the sixties [51,65–71]. Decreasing the surface area by high-temperature calcination affects not only the surface area but also the porosity and pore structure of the material. Fig. 2 illustrates how high-temperature calcination has affected mechanical strength (attrition), pore volume, surface area, and average pore diameter for the supports used to prepare most of the catalysts

(No. 1–8 and 15–21) detailed in Table 1. It is worth noting that the precursor for all these supports is the γ-Al_2O_3 (Puralox SCCa-45/190, 178 m^2/g), also shown in the plots. The increased mechanical strength for the 5 wt% Ni- and 10 wt% Mg-modified supports (Fig. 2a) is likely related to how the spinel inclusions bind together the α-Al_2O_3 phase (grains). The spinel inclusions also decrease the overall pore volume as compared to the pure α-Al_2O_3 (Fig. 2a), while retaining slightly more of the surface area of the starting material (Fig. 2b, Table 1). It also appears that a higher loading of spinel (10 wt% Mg vs. 5 wt% Ni) better prevents the narrower pores in the γ-Al_2O_3 from collapsing completely during high-temperature calcination (>1400 K), as illustrated in Fig. 2c. The preparation procedure was not optimized, so there is likely room for improvements with respect to retaining more of the surface area and pore volume of the starting material in the spinel-strengthened supports. Typically, the impregnation and low-temperature calcination of Co (+Re) on the supports increases the attrition values very slightly, as previously shown for 20 wt% Co/γ-Al_2O_3 [51], but it is the high-temperature calcination of the support that has the dominating influence on the mechanical strength. Therefore, only attrition values for the supports are presented here. A follow-up on Rytter et al. [51] with more attrition values for supports and catalysts will be published later. Other effects related to changing the calcination rate, the number of calcinations, and reductions, as well as the support acidity, have been addressed extensively in the literature [16,25–30]. Co(Re) supported on α- and γ-Al_2O_3 have previously been characterized with scanning transmission electron microscopy (STEM) [22], and 3D images from STEM tomography have been published for CoRe supported on γ-Al_2O_3 and Ni-spinel; $NiAl_2O_4$ (5 wt% Ni) [72].

3.2. Catalyst reducibility, dispersion, and cobalt particle sizes

There is no doubt that Fischer–Tropsch synthesis requires activation of the catalyst by exposing it to a reducing atmosphere. The presence of reduced sites is imperative to dissociative H_2 adsorption on transition metals for FTS [73]. Hydrogen atoms may also spill over to the support [74], thus providing a support-dependent reservoir. Because the unreduced catalyst is inactive for FTS, the degree of reduction becomes an important parameter for maximizing FTS productivity (throughput).

In order to increase the dispersion of a catalyst, using a high surface area support may seem like a good idea. However, as illustrated in Fig. 3a, when using the *incipient wetness* impregnation technique, with nitrate-based precursors dissolved in water, there appears to be a limit with respect to catalyst dispersion; leveling out around 10% (about 10 nm particles) with the drying and calcination procedure used here. Higher dispersions (down to 3–5 nm particles) can be achieved by using, e.g., deposition–precipitation [75–77], where aqueous cobalt amine carbonate complexes are decomposed at 333–383 K. Another alternative for increasing dispersion, tuning particle sizes, and their distribution is by reduc-

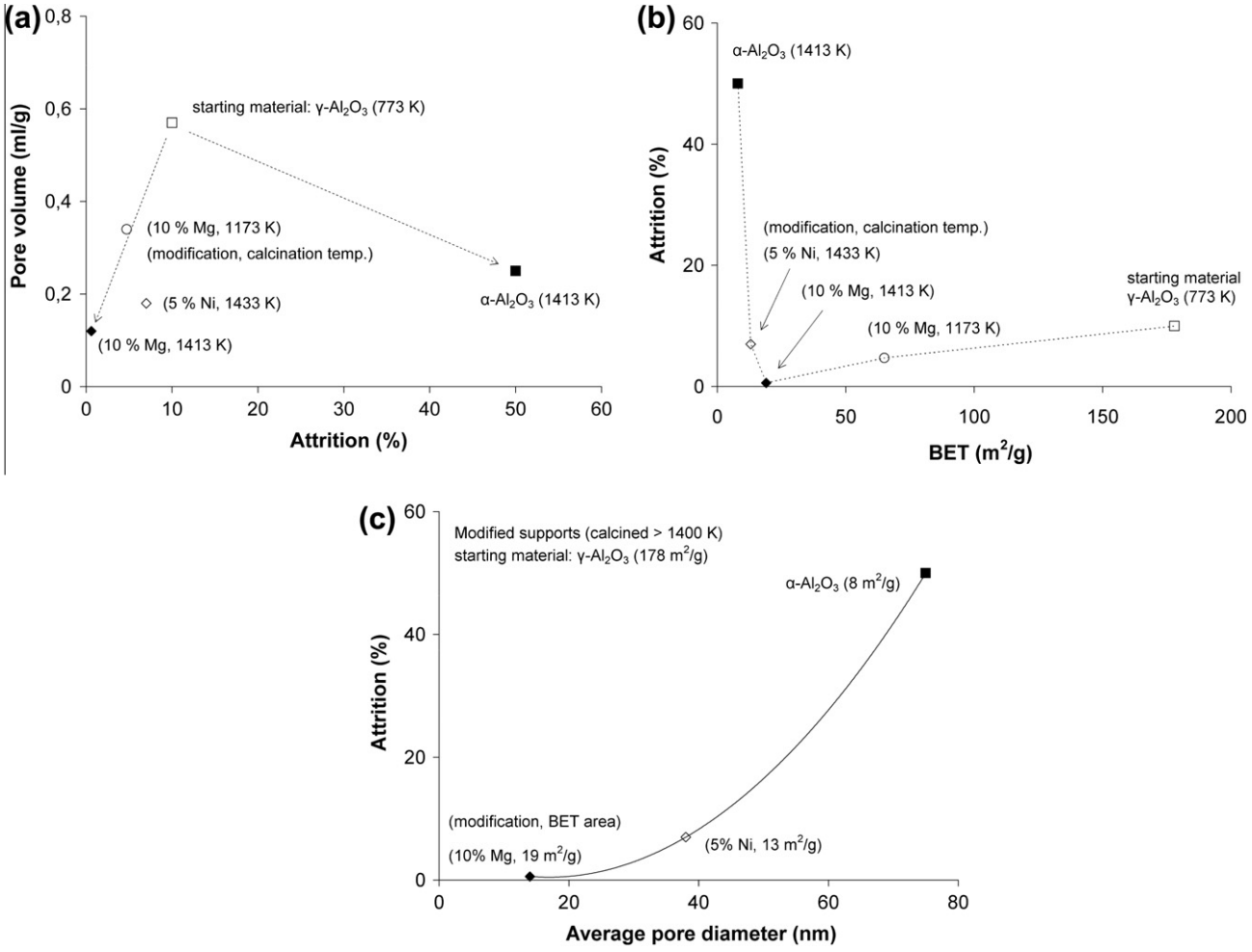

Fig. 2. Illustration of attrition [51] correlated to (a) pore volume, (b) BET surface area, and (c) average pore diameter for the following support materials; γ-Al_2O_3 (□), α-Al_2O_3 (■), $NiAl_2O_4$-α-Al_2O_3 (◇), $MgAl_2O_4$-α-Al_2O_3 (♦), and 10%Mg-γ-Al_2O_3 (○).

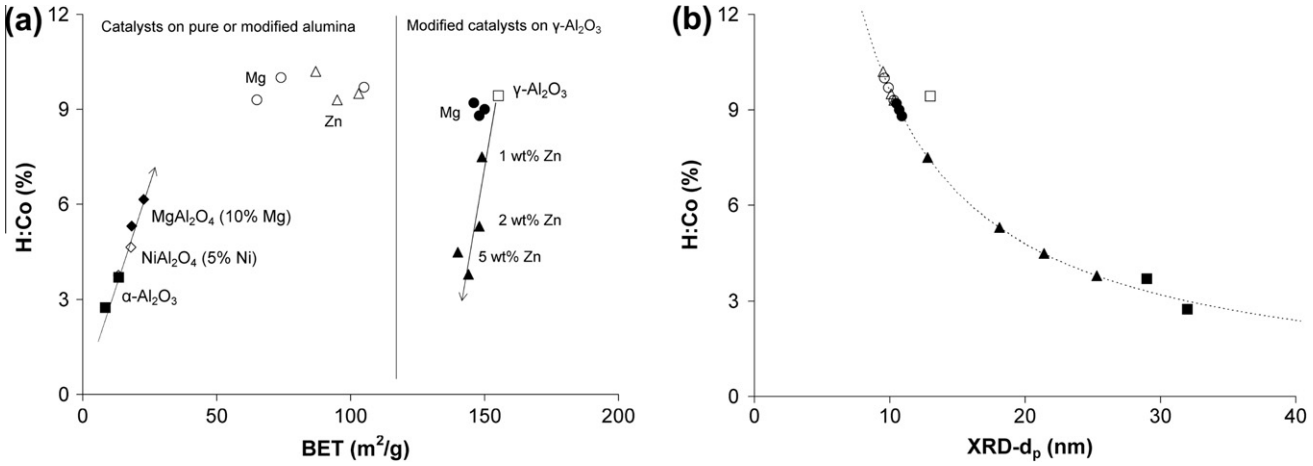

Fig. 3. *Ex situ* hydrogen chemisorption as a function of; (a) BET surface area for different 12 wt% Co catalysts, most of which are promoted by 0.5 wt% Re, and (b) cobalt particle size from XRD. Support materials; γ-Al_2O_3 (□), α-Al_2O_3 (■), $NiAl_2O_4$-α-Al_2O_3 (◇), $MgAl_2O_4$-α-Al_2O_3 (◆), Mg-γ-Al_2O_3 (○), Zn-γ-Al_2O_3 (△), and γ-Al_2O_3, where Co/Re was co-impregnated with Mg (●) or Zn (▲). See Table 1 for details.

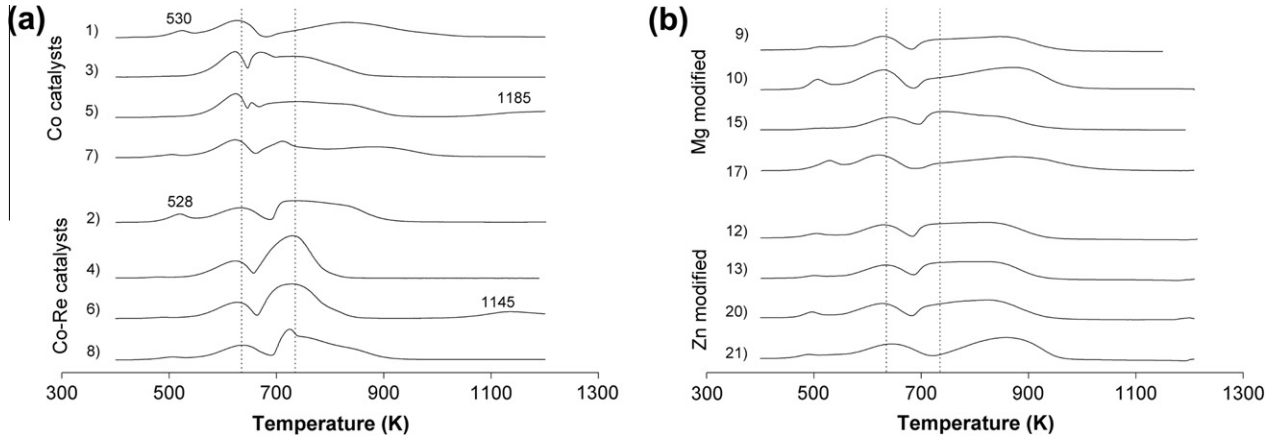

Fig. 4. Temperature-programmed reduction of 12 wt% Co (+0.5 wt% Re) catalysts (0.2 g) using 7% H_2 in Ar, heated at 10 K/min. Comparing: (a) Co and Co-Re catalysts on different supports; γ-Al_2O_3 (No. 1 and 2), α-Al_2O_3 (No. 3 and 4), $NiAl_2O_4$-α-Al_2O_3 (No. 5 and 6) and $MgAl_2O_4$-α-Al_2O_3 (No. 7 and 8), and b) catalysts with Mg or Zn added to the γ-Al_2O_3 support and calcined (1173 K) prior to impregnation with Co–Re (No. 9, 10, 12 and 13) or co-impregnated with Co-Re (No. 15, 17, 20 and 21), all numbered according to Table 1. The two dotted lines: 635 K and 735 K.

tion of nitrate precursors with small amounts of NO in an inert carrier gas [78–80] or by using other solvents than water, such as ethylene glycol [41,81]. For intermediate cobalt dispersion (D), values the metal particle (d_p) size can be estimated by a formula that is close to d_p (nm) = 96/D (%) [56]. Fig. 3b correlates H:Co, which is an estimate for D, with particle sizes from XRD. The dotted line is simply a plot of the $d_p = 96/D$ formulae. Table 1 also confirms that H_2 chemisorption and XRD yield more or less the same particle size for all catalysts with 12 wt% Co (+0.5 wt% Re). Co-impregnating Co–Re with Zn (▲) had a clear loading-dependent negative effect on dispersion, yielding increased Co particle sizes, as seen from both Fig. 3a and b as well as Table 1.

The catalyst reducibility and degree of reduction (DOR) were investigated by temperature-programmed reduction (TPR) and O_2 titration. Table 1 summarizes the DOR values obtained for the first two sections of catalysts using oxygen titration. No DOR values were obtained for the other two sections, but the TPR profiles and areas underneath are similar to those for catalysts No. 1 and 2 on γ-Al_2O_3. Borg et al. [21,82] and Khodakov et al. [35] have found that oxygen titration likely underestimates the extent of reduction, probably due to incomplete oxidation because of the relative high stability of CoO in inert atmosphere above 623 K [83]. Comparing the DOR values here to those from Borg et al. [21] (having used the same equipment and procedure), we expect the actual degree of reduction to be higher than the DOR values from oxygen titration. DOR values are most likely about 25–30% higher than the values from O_2 titration, and thus in the range of 85–100%, when including all catalysts in Table 1 together.

In Fig. 4, TPR profiles are illustrated for most of the catalysts in Table 1. Borg et al. demonstrated that the peak located at about 510–530 K is from the reduction of residual nitrate [21]. Hydrogen spillover has previously been suggested as the mechanism by which Re promotes the reduction of CoO to Co^0 [84]. A more recent investigation by low-energy ion scattering [85] indicates that rhenium preferentially occupies sub-surface sites within bimetallic Co–Re clusters. The results were supported by density functional theory (DFT) calculations on small clusters (Co_{14}, $Co_{13}Re$, $Co_{12}Re_2$). TPR data suggested the following reduction sequence: $Co_3O_4 \rightarrow CoO$, then $Re_2O_7 \rightarrow Re^0$, and finally $CoO \rightarrow Co^0$, but the dynamics of how rhenium relocates to the sub-surface layers was not possible to determine from the data set. The two-step reduction sequence $Co_3O_4 \rightarrow CoO \rightarrow Co^0$ has previously been verified in EXAFS studies [30,82]. Our results also show that Re had no noticeable effect on the first step of the reduction process, from Co_3O_4 to CoO

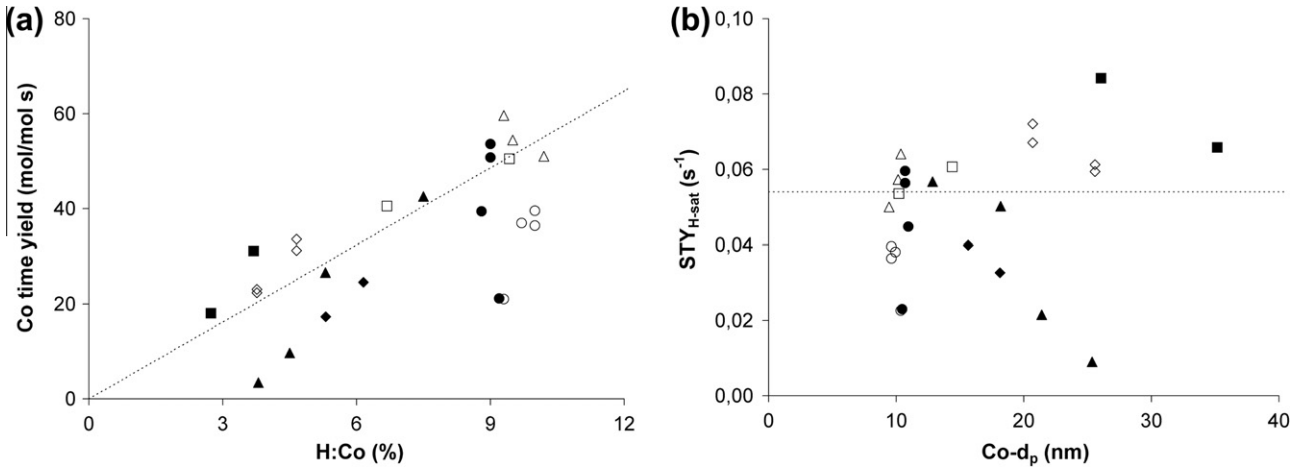

Fig. 5. Initial reaction rates from Fischer–Tropsch synthesis at 483 K, 20 bar and $H_2/CO = 2$, obtained after 8 h on stream. (a) Cobalt-time yield (Co.t.y.) as a function of H:Co (%) and (b) site-time yield (STY) as a function of Co particle size from H_2 chemisorption. Illustrating different 12 wt% Co catalysts, most of which are promoted by 0.5 wt% Re. Support materials; γ-Al_2O_3 (□), α-Al_2O_3 (■), $NiAl_2O_4$-α-Al_2O_3 (◇), $MgAl_2O_4$-α-Al_2O_3 (◆), Mg-γ-Al_2O_3 (○), Zn-γ-Al_2O_3 (△) and γ-Al_2O_3, where Co/Re was co-impregnated with Mg (●) or Zn (▲). The dotted line identifies the standard catalyst (No. 2): Co-Re/γ-Al_2O_3.

(the peak located near the dotted line at 635 K), in agreement with previous studies [38,84]. The exact nature of the TPR signal from the second reduction step is probably affected by how different particle sizes (Co loading) interact with the support [19]. Comparing catalysts No. 1, 3, 5, and 7 from Fig. 4a supports this view. The TPR signal for the more highly dispersed catalysts (d_p = 14, 35, 26, and 18 nm, respectively) is stretched out to higher temperatures. Such an effect was also noted by Borg et al. [21] for a series of Co on different gamma-aluminas. For catalysts on the Ni-spinel modified support (No. 5 and 6), there is also a high temperature peak (>1120 K), which is related to the reduction of the spinel [52]. Reduction of $CoAl_2O_4$ requires comparably high temperatures [86]. From the TPR profiles, the catalysts on the Mg-spinel-modified supports (No. 7 and 8) appear slightly more difficult to reduce than those on the Ni-spinel-modified supports (No. 5 and 6), which is also in agreement with the DOR values in Table 1. Because the loading of Mg is higher (10 wt%) than the loading of Ni (5 wt%), it is not unlikely that this may have had an effect.

The TPR profiles in Fig. 4b are largely comparable to the catalysts on γ-Al_2O_3 (No. 1 and 2) in Fig. 4a. At higher loadings of Mg or Zn ($\geqslant$1%), the reduction of CoO to Co^0 shifts slightly toward higher temperatures, most clearly seen for 5 wt% Mg (No. 10) or 5 wt% Zn (No. 21). This may suggest interactions between ZnO or MgO and CoO. MgO or ZnO were not observed in the XRD data, indicating that these phases are either highly dispersed or lack crystallinity. Zhang et al. [33], who studied 15 wt% Co/MgO/Al_2O_3 catalysts with different loadings of MgO, reported the same effect on reducibility during TPR, as described here. They attributed this negative effect to the formation of a solid solution (single phase) MgO–CoO. The formation of solid solutions with ZnO–CoO is also known from the literature [87–89].

3.3. Effects on activity from modifications

It has been repeatedly shown in the literature that for particle sizes >5–7 nm, the activity apparently correlates to the cobalt surface area measured by H_2 chemisorption [4,7,90]. In Fig. 5a, initial cobalt-time yields are illustrated for 12 wt% Co catalysts, most of which have been promoted by 0.5 wt% Re. The dotted line identifies the standard Co-Re/γ-Al_2O_3 catalyst (No. 2, Table 1), which serves as a good reference point. The catalysts below this line have all been modified with $\geqslant$0.1 wt% Mg or Zn, either as a modification of the support prior to high-temperature calcination ($\geqslant$1173 K) followed by impregnation of Co–Re or co-impregnated with Co and Re. If these catalysts were not included in Fig. 5a, then the general trend is that the cobalt-time yield correlates linearly to the amount of hydrogen adsorbed during chemisorption, here divided by the nominal loading of cobalt to obtain H:Co (%). As seen from Table 1, there was excellent agreement between estimates of particle sizes from H_2 chemisorption and XRD. A particle size or dispersion effect can, therefore, be excluded as an explanation for this poisonous effect of Mg and Zn. Neither can the effect be explained by *ex situ* differences in reducibility based on TPR. The results strongly suggest a chemical/site poisoning effect, perhaps most comparable to the effect of other alkalis [91]. However, *in situ* differences in degree of reduction when exposed to H_2/CO cannot be excluded without further studies.

In general, we found that the effect of Re was in accordance with previous studies [24,38,84], promoting the reduction and dispersion of cobalt. Fig. 5b illustrates site-time yield (STY) as a function of cobalt particle size, calculated using a formula that can be rounded off to d_p (nm) = 96/D (%) [56], where H:Co (%) is used as an estimate for D (%). The solid line is only suggestive, as there are no results here for particles <9 nm, but this indication is in line with results from the literature [2–4]. Again, as in Fig. 5a, the catalysts that have been modified with $\geqslant$0.1 wt% Mg or Zn are below the dotted line, confirming that Mg and Zn appears to have a poisoning effect on initial catalytic activity, as the results cannot be explained by dispersion or particle size effects. The effect appears to depend on loading and whether Mg or Zn was added to the support and then calcined at high temperatures ($\geqslant$1173 K) prior to impregnation with Co–Re, or co-impregnated with Co and Re. The cobalt-time yield for catalyst No. 10 (Table 1), where 5 wt% Mg was added to the support is comparable to catalyst No. 16, where 0.1 wt% Mg was co-impregnated together with Co and Re. The same is true for catalysts No. 11 and 17, with 10 wt% Mg and 1 wt% Mg, respectively. It cannot be excluded that the nature of the Mg species may be different on these catalysts, but the effect is likely related to the different degrees of interaction achieved by sequential impregnation and calcination in between, compared to co-impregnation. Interestingly, there was no significant negative effect on activity from Zn, when added to the support and then high-temperature calcined (1173 K) prior to impregnation with Co–Re. In contrast, 5 wt% Zn co-impregnated with Co–Re was extremely poisonous to activity, as indicated by the two points (▲) with STY $\leqslant$0.02 s^{-1}. These two catalysts had insufficient activity

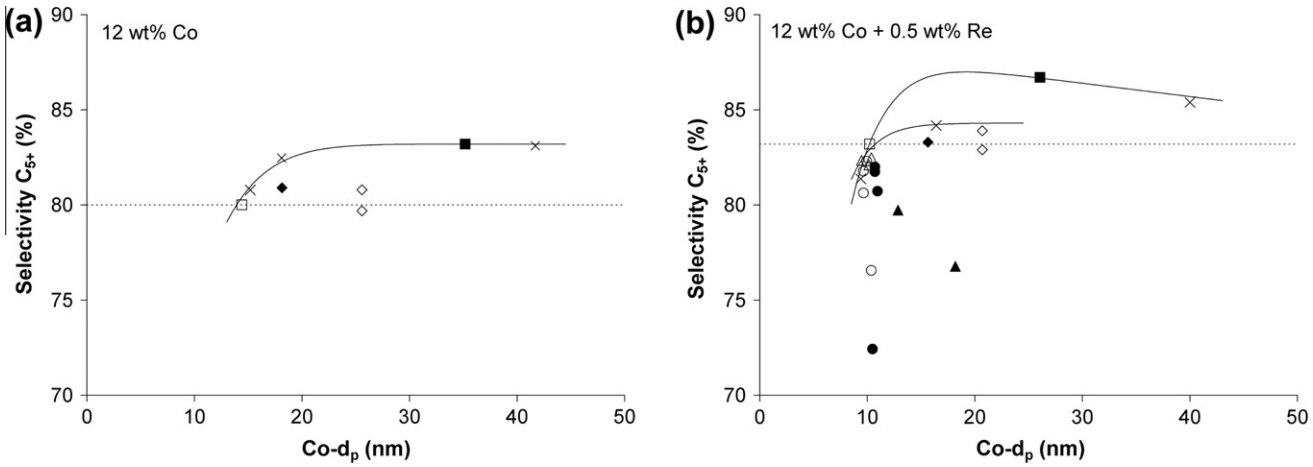

Fig. 6. Selectivity to long-chain hydrocarbons (C_{5+}) obtained at 45–55% CO conversion (extrapolated to 50% CO conversion) during Fischer–Tropsch synthesis at 483 K, 20 bar and $H_2/CO = 2$, illustrated as a function of Co particle size for catalysts with a) 12 wt% Co and b) 12 wt% Co + 0.5 wt% Re. Support materials; γ-Al_2O_3 (□), α-Al_2O_3 (■), $NiAl_2O_4$-α-Al_2O_3 (◇), $MgAl_2O_4$-α-Al_2O_3 (◆), Mg-γ-Al_2O_3 (○), Zn-γ-Al_2O_3 (△) and γ-Al_2O_3, where Co/Re was co-impregnated with Mg (●) or Zn (▲). Data from Storsæter et al. [99] for catalysts on γ-Al_2O_3, SiO_2 and TiO_2, extrapolated to 50% CO conversion (×). The dotted line identifies the catalysts (No. 1 and 2) on γ-Al_2O_3.

for adjusting the gas velocity to reach high CO conversion. For catalysts No. 20, the initial CO conversion was <2% after 24 h, and for catalyst No. 21, it reached at maximum of 5.6% CO conversion after 74 h. Neither could be adjusted to 50% CO conversion and are, therefore, not included in Sections 3.4–3.6.

A variation of up to 1 K in bed temperature corresponds in experimental uncertainty of STY = 0.065 ± 0.004 s^{-1}, when assuming that the activation energy in Eq. (4) is E_a = 130 kJ/mol, using recent estimates for the rate-limiting step in model studies [92,93]. R is the ideal gas constant, and T is the bed temperature. The measured experimental variation in bed temperature was typically <1 K. The difference between 0.054 s^{-1} for Co–Re/γ-Al_2O_3 (No. 2) and 0.084 s^{-1} for Co–Re/α-Al_2O_3 (No. 4) corresponds to as much as 7 K if converted into a temperature difference. Thus, variation in bed temperature is unlikely to be the only reason for this difference in STY. *In situ* measurements of the number of active sites and concentrations of surface species will be necessary to address this issue in further detail.

$$\mathrm{STY}_1/\mathrm{STY}_2 = e^{-\frac{E_a}{R}\left(\frac{1}{T_1}-\frac{1}{T_2}\right)} \quad (4)$$

3.4. Effects on selectivity from modification

The FTS carbon selectivity can be described by polymerization kinetics, where different chain termination or chain propagation probabilities can be identified for each of the pathways in Fig. 1, where, e.g., $r_p = k_p \cdot \exp(-E_a/RT)$. These pathways are influenced by both catalyst and operating conditions [27]. Thus, by introducing modifications, the carbon selectivity may be affected through structural and/or site/kinetic effects.

In Fig. 6a, the selectivity to C_{5+} at 50% CO conversion is illustrated for the 12 wt% Co catalysts from Table 1, as well as for the 12 wt% Co catalysts on γ-Al_2O_3, SiO_2 and TiO_2 from Storsæter et al. [22]. The solid line is only suggestive and added as a reading aid. The dotted line identifies the Co/γ-Al_2O_3 reference catalyst (No. 1). There are two ways to read this plot, either being largely in agreement with constant selectivity for particles >6–8 nm [2,4] or in agreement with increasing C_{5+} selectivity with increasing particle size, as previously reported for the range 10–15 nm [21]. Because the studies that showed constant C_{5+} selectivity for particles >6–8 nm were done on carbon nanofiber-supported catalysts, thus avoiding the issue with possible effects from the pore structure of the support, we believe the apparent increased selectivity to C_{5+} with increasing particle size in Fig. 6a is an effect related to the local conditions created within the support rather than a site/kinetic effect. To further explore this point of view, a range of catalysts with different Co particle sizes in the range 10–40 nm on different pure low surface aluminas (5–50 m^2/g) would be very interesting as a future study. Compared to the catalyst on γ-Al_2O_3, the Ni-spinel-modified support does not appear to have improved the conditions for increased C_{5+} selectivity to the same extent as the might be indicated by the Co particle size obtained by incipient wetness impregnation. Also when compared to the results on carbon nanofiber supports, showing of constant selectivity for particles >6–8 nm [2,4], the Ni-spinel appears to have had no negative effect on C_{5+} selectivity. However, the relatively modest C_{5+} selectivity of the Ni-spinel-based catalyst in this work is surprising, as our previous studies [50,51] have demonstrated significantly higher C_{5+} selectivity over Ni-spinel-based catalysts than over γ-Al_2O_3-based catalysts.

A positive effect of Re on C_{5+} selectivity is seen by comparing catalysts on identical supports from Fig. 6a and b. This was expected [22,24,38,94]. Again, the dotted line identifies the reference catalyst, No. 1 and 2, respectively, in Fig. 6a and b. Almost all the catalysts in Fig. 6b that fall below this line are catalysts that have been modified with Mg or Zn. Their effect on C_{5+} selectivity is loading dependent, as previously seen for activity in Fig. 5b, and also depends on whether Mg or Zn was added to the support and then calcined at high temperatures ($\geqslant$1173 K), prior to impregnation with Co–Re, or co-impregnated together with Co and Re. This loading dependency is explored in more detail later.

Another interesting aspect of Fig. 6b is suggested by the solid line tracing unmodified 12 wt% Co + 0.5 wt% Re catalysts on γ-Al_2O_3 and α-Al_2O_3 reported here and the TiO_2-supported catalyst reported by Storsæter et al. [22]. The solid line suggests that there may be an optimum particle size for this specific Co/Re ratio, where the promotion of Co with Re yields maximum C_{5+} selectivity. Fig. 6b suggests that this may be somewhere between 10 and 20 nm for 12 wt% Co + 0.5 wt% Re. Borg et al. [41] also suggested an optimum particle size for Co on different aluminas; however, considering the results on carbon nanofiber [2,4], this apparent optimum may indicate a support-related effect. An effect on selectivity related to Co/Re ratio is not new [24], but with respect to selectivity, it is critically important to compare catalysts at the same CO conversion level [21]. This idea of an optimum particle

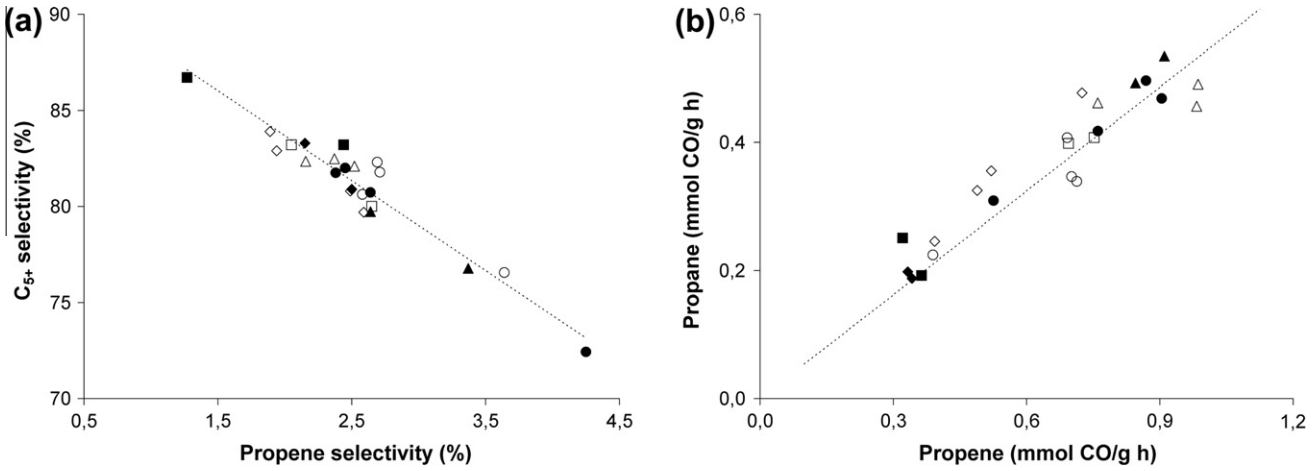

Fig. 7. Results from Fischer–Tropsch synthesis obtained at 45–55% CO conversion (extrapolated to 50% CO conversion) during Fischer–Tropsch synthesis at 483 K, 20 bar and $H_2/CO = 2$. Illustrating for different 12 wt% Co catalysts, most of which are promoted by 0.5 wt% Re; a) C_{5+} selectivity as a function of propene selectivity and b) rate of propane (C_{3-}) formation as a function of rate of propene ($C_{3=}$) formation. Support materials; γ-Al_2O_3 (□), α-Al_2O_3 (■), $NiAl_2O_4$-α-Al_2O_3 (◇), $MgAl_2O_4$-α-Al_2O_3 (♦), Mg-γ-Al_2O_3 (○), Zn-γ-Al_2O_3 (△) and γ-Al_2O_3, where Co/Re was co-impregnated with Mg (●) or Zn (▲).

size for a specific Co/Re ratio would be interesting to follow up in another study, as it relates to whether the effect of Re is only to disperse Co or if it has a chemical/site effect as well. So far, the Co particle size effect has only been firmly established for catalysts without Re on carbon nanofiber [2,4].

Re-adsorption and insertion of alkenes into the growing hydrocarbon chain has been considered one possible explanation for increased C_{5+} selectivity [7,27]. Fig. 7a illustrates one perspective, from which it may be easy to jump to such a conclusion. If the effect of Re was to promote the re-adsorption of alkenes such as propene and incorporate this into C_{5+} products, we would expect a lower propene/propane ratio for Re-promoted catalyst. Rytter et al. [95] recently demonstrated that the olefin/paraffin (o/p) ratio for C_3, as well as for C_4 and C_5, is fairly constant and largely independent of support, but depends strongly on CO conversion, as olefin hydrogenation is known to be inhibited by water (formation), as shown for propene hydrogenation [96]. In Fig. 7b, the rate of propane formation is illustrated as a function of the rate of propene formation for all 12 wt% Co (+0.5 wt% Re) catalysts at 50% CO conversion. The dotted line identifies the Co-Re/γ-Al_2O_3 reference catalyst (No. 2), with an o/p ratio of 1.85. There is some variation in o/p ratio depending on support material and catalyst preparation, ranging from 1.3 on the α-Al_2O_3, perhaps suggesting a higher degree of re-adsorption with this wide-pored support (Fig. 2c), to 2.1 on some (but not all) of the Mg- and Zn-modified catalysts, perhaps suggesting some inhibition of re-adsorption. No correlation was found between Mg loading and o/p ratio of C_3. The same was true for C_4, while for C_5 and C_6, the o/p ratio increased very slightly with increasing Mg loading for the catalysts with Mg co-impregnated with Co and Re. For Mg added to the support (catalyst No. 9–11), no correlation between loading and o/p ratio could be found. Increasing levels of Zn (1–10 wt%) added to the support prior to high-temperature calcination (catalyst No. 12–14) had the opposite effect, with very slightly decreasing o/p ratio (carbon numbers C_3–C_6) with increasing loading of Zn. Higher carbon numbers were not analyzed. The experimental uncertainty was significant, e.g., with C_3 o/p values of 1.7–2.0 obtained during repeated trials on catalyst No. 10. The o/p ratio for C_4–C_6 was in general found to increase slightly at steady-state operating conditions (during 24+ hours), thus the experimental uncertainty is particularly high for this fraction. Some of the variations may be caused by diffusion effects related to pore structure, pellet size, and possibly bed packing including inert/catalyst mixing [95]. Rytter et al. [95] also demonstrated that the o/p ratio increases with decreasing

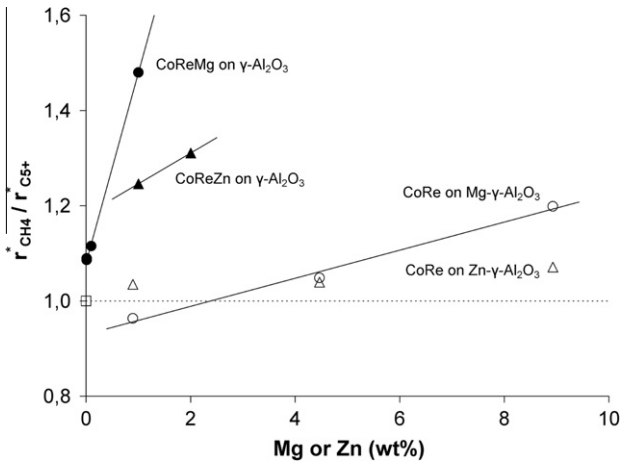

Fig. 8. Results from Fischer–Tropsch synthesis obtained at 45–55% CO conversion (extrapolated to 50% CO conversion) during Fischer–Tropsch synthesis at 483 K, 20 bar and $H_2/CO = 2$. Illustrating for catalysts with 12 wt% Co and 0.5 wt% Re the ratio between normalized reaction rates according to Eq. (5) as a function of modification level (wt%). Support materials; γ-Al_2O_3 (□), Mg-γ-Al_2O_3 (○), Zn-γ-Al_2O_3 (△) and γ-Al_2O_3, where Co/Re was co-impregnated with Mg (●) or Zn (▲).

pellet size, indicating that olefins dominate the primary FTS product and that paraffins are to a large extent formed by secondary hydrogenation or cracking followed by hydrogenation, r_s and r_c, respectively (Fig. 1). Given the near to constant o/p ratio seen in Fig. 7b, this leads to the conclusion that the effect of Re on selectivity is most likely related to a chemical (site) effect [38,85], likely through influencing surface concentrations ($H^*/CO/C^*_n$) and modifying the binding energy of surface species, two effects that are not independent.

Returning to the loading-dependent effect of Mg and Zn modifications, in Fig. 6b, all catalysts from this study below the dotted line were modified with either Mg or Zn. Studying Table 1, comparing the reference catalyst Co–Re/γ-Al_2O_3 (No. 2) to catalysts with Zn (No. 12–14 and 18–21), the effect of Zn on activity (r_{CO}) and selectivity (CH_4, C_{5+}) was small when added to the support prior to high-temperature calcination (1173 K) followed by impregnation of Co–Re (No. 12–14). However, the negative effect was significant and increasing with loading when co-impregnated with Co–Re (No. 18–21). The activity of catalysts with 5 wt% Zn co-impreg-

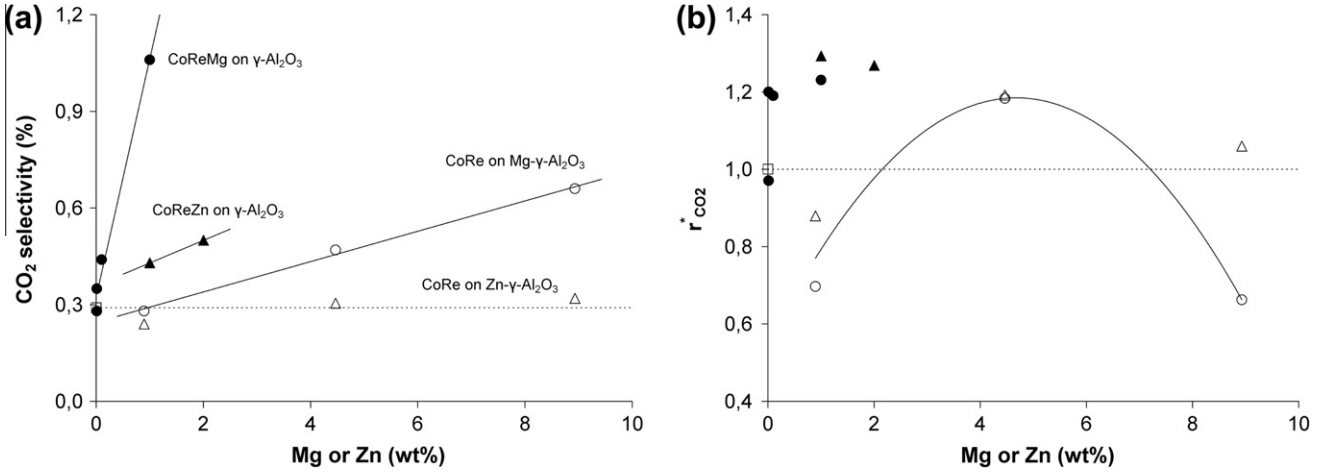

Fig. 9. (a) Selectivity to CO_2 and (b) reaction rate to CO_2 relative to the reference catalyst (No.2, □), illustrated as a function of modification level (wt%) for 12 wt% Co + 0.5 wt% Re catalysts, obtained at 45–55% CO conversion (extrapolated to 50% CO conversion) during Fischer–Tropsch synthesis at 483 K, 20 bar and $H_2/CO = 2$. Support materials; γ-Al_2O_3 (□), Mg-γ-Al_2O_3 (○), Zn-γ-Al_2O_3 (△) and γ-Al_2O_3, where Co/Re was co-impregnated with Mg (●) or Zn (▲).

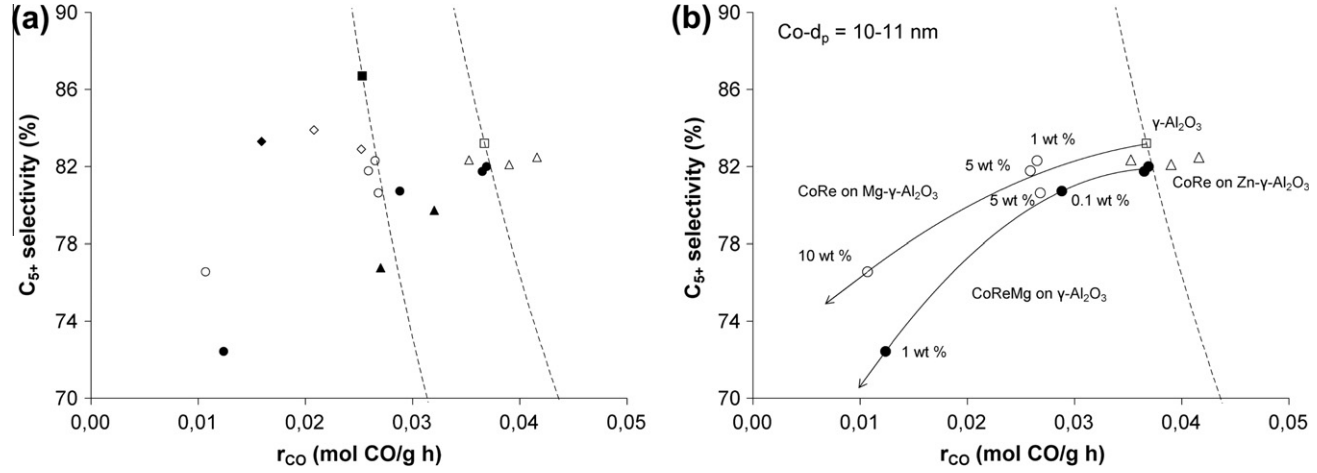

Fig. 10. Selectivity to C_{5+} as a function of the rate of reaction (mol/g h) obtained at 45–55% CO conversion (extrapolated to 50% CO conversion) during Fischer–Tropsch synthesis at 483 K, 20 bar and $H_2/CO = 2$. Illustrating (a) all 12 wt% Co + 0.5 wt% Re catalysts and (b) only 12 wt% Co + 0.5 wt% Re, where the cobalt particle size determined from H_2 chemisorption was 10–11 nm. The two stipled lines are productivity lines along which the C_{5+} yield ($Y_{C5+} = r_{CO} \cdot S_{C5+}$) is constant and identify the γ-Al_2O_3-and α-Al_2O_3-supported catalysts. Support materials; γ-Al_2O_3 (□), α-Al_2O_3 (■), $NiAl_2O_4$-α-Al_2O_3 (◇), $MgAl_2O_4$-α-Al_2O_3 (◆), Mg-γ-Al_2O_3 (○), Zn-γ-Al_2O_3 (△) and γ-Al_2O_3, where Co/Re was co-impregnated with Mg (●) or Zn (▲).

nated with Co–Re was too low to be adjusted to 50% CO conversion. For catalysts modified with Mg (No. 9–11 and 15–17), the negative effect on activity (r_{CO}) and selectivity (CH_4, C_{5+}) was significant and increasing with loading for all catalysts. Again, the effect was stronger when co-impregnated with Co–Re (No. 15–17) than when added to the support prior to high-temperature calcination (1173 K) followed by impregnation of Co–Re (No. 9–11). Summarizing, it appears that both Mg and Zn can affect catalytic activity and both shifts the selectivity toward a lighter product, suggesting modification of chain propagation versus hydrogenation activity. In order to compare the relative effect of Mg and Zn on reaction rates, the rates of CH_4 and C_{5+} formation for the modified catalysts were divided by the respective rates of the reference catalysts (No. 2), as according to Eq. (5).

$$\frac{r^*_{CH_4}}{r^*_{C_{5+}}} = \frac{r_{CH_4}/r^{ref}_{CH_4}}{r_{C_{5+}}/r^{ref}_{C_{5+}}} \quad (5)$$

The results from Eq. (5) were plotted in Fig. 8. When this ratio is >1.0, the rate of C_{5+} formation (chain propagation) has been more strongly affected by modifications than the rate of CH_4 formation (methanation, hydrogenation). Thus, from Fig. 8, it appears that Mg or Zn has been more detrimental to chain propagation than to hydrogenation (methanation) activity. The effect is substantially stronger when Mg or Zn is co-impregnated with Co–Re than when added to the support and high-temperature calcined (1173 K) before impregnating with Co–Re. This difference in how the modification influences chain propagation versus hydrogenation/methanation may suggest that there is more than one type of active sites, and that, these are not all affected to the same extent by Mg or Zn.

3.5. Effects on water–gas-shift from modification

It is well known that Co catalysts are not very active for water–gas-shift (WGS) [16], and thus requires a higher H_2/CO ratio than Fe catalysts in order to avoid H_2 depletion at high CO conversions. When operating with natural gas-based syngas at $H_2/CO = 2$, low WGS activity is desirable, since the formation of CO_2 constitutes a loss of carbon. On the other hand, considering operation of Co catalysts based on biosyngas or syngas from coal, adding a WGS

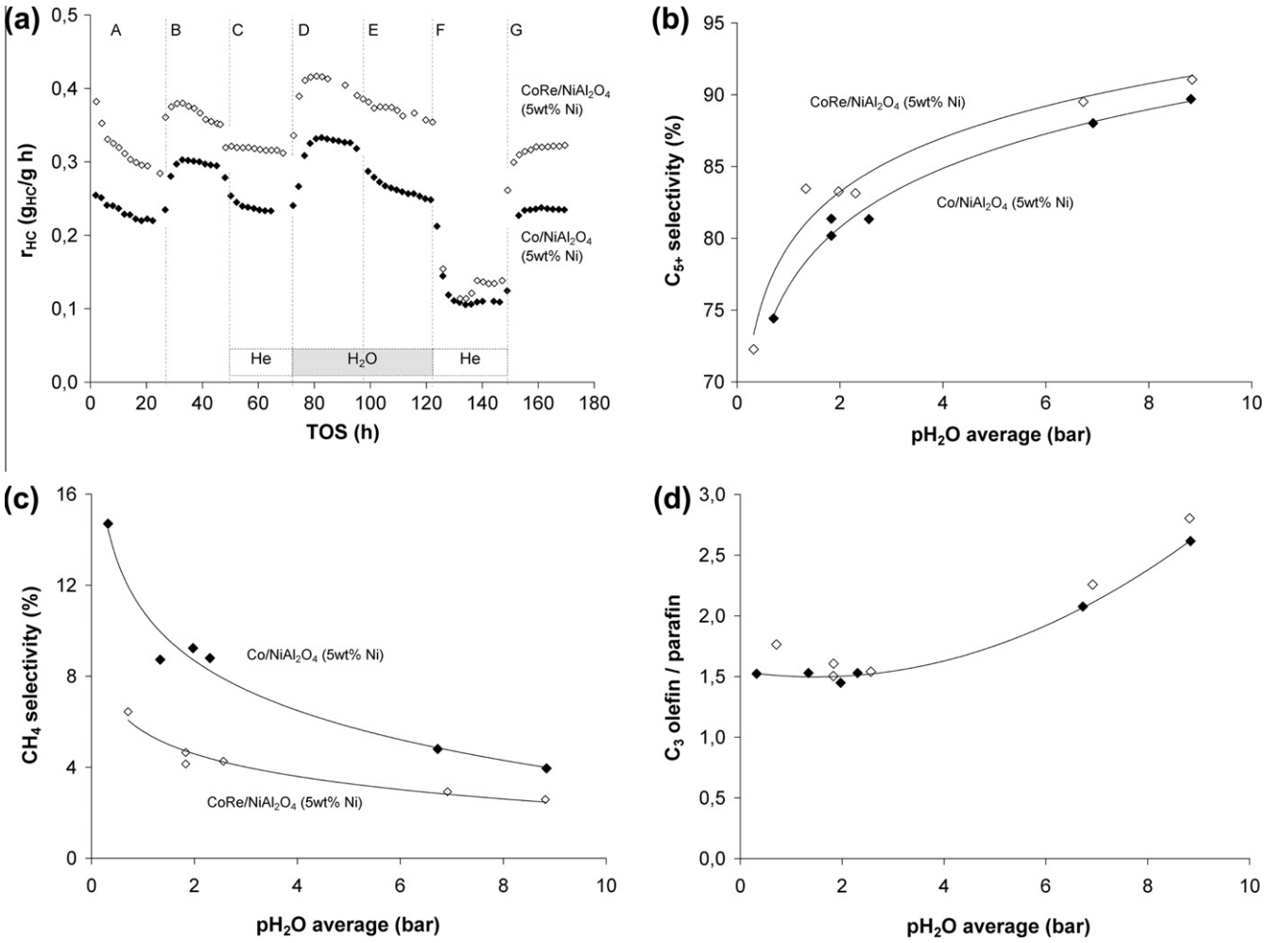

Fig. 11. Illustrating results from Fischer–Tropsch synthesis for $NiAl_2O_4$-α-Al_2O_3-supported catalysts as a function of time on stream at 483 K, 20 bar and H/CO = 2 during different periods: A: initial conditions, B: after adjusted gas feed to 50% CO conversion, C: with 5 bar He, D: with 4 bar H_2O, E: with 6.9 bar H_2O, F: with 10 bar He and G: same feed as in B. Illustrating for 12 wt% Co (♦) and 12 wt% Co + 0.5 wt% Re (◇) (a) hydrocarbon production rates, and as a function of average H_2O partial pressure; (b) C_{5+} selectivity, (c) CH_4 selectivity and (d) C_3 olefin/paraffin ratio.

step, increasing *in situ* WGS activity or co-feeding additional H_2 will be necessary to avoid its conversion depletion. A separate WGS step can be combined with CO_2 capture prior to FTS and is, therefore, a more likely commercial alternative if CO_2 has to be captured, thus adding *in situ* WGS activity is generally not desirable.

In Fig. 9a, the selectivity to CO_2 is illustrated as a function of Mg or Zn loading. Again, the difference with respect to adding Mg or Zn to the support prior to high-temperature calcination (1173 K) and then impregnating with Co-Re, compared to co-impregnating Mg or Zn with Co–Re, is very significant. Adding Zn to the support (△) had no effect on CO_2 selectivity, while the other modifications all increased selectivity to CO_2. However, increased selectivity to CO_2 does not necessarily imply increased WGS activity. In Fig. 9b, the relative effect of Mg or Zn on the rate of CO_2 formation illustrates that WGS activity is actually modified with up to as much as 30%, when compared to the reference catalyst (No. 2, □), also identified by the dotted line. For the catalysts where Mg or Zn has been added to the support prior to high-temperature calcination (1173 K), the relative effect on WGS activity appears to go through a maximum at 5 wt% modification, and again the effect of Mg or Zn is much stronger when co-impregnated with Co–Re. From a commercial perspective, CO_2 formation is generally not desirable and only increases the amount of inert in the recycle stream (or flue gas). Thus, decreasing WGS activity may be more desirable than increasing it. Adding small amounts of Mg or Zn to the support and calcining at high temperatures (1173) is slightly beneficial with respect to this, but due to loss in overall activity and C_{5+} selectivity, in particular Mg, is likely better avoided.

3.6. Fischer–Tropsch C_{5+} yield

With respect to commercialization of a catalyst, the yield and stability (life-time) are very important overall success parameters. In Fig. 10, the C_{5+} selectivity is illustrated as a function of the reaction rate (r_{CO}). The product of these two parameters determines the FT C_{5+} yield. With respect to maximizing yield, the most desirable catalysts will be located toward the upper right corner in Fig. 10a. However, the C_{5+} yield, here illustrated after about 50 h, needs to be balanced with evaluations of mechanical strength and long-term deactivation rates, which have not been investigated here. Also, costs related to the recycle of light products must be considered when choosing the optimal catalyst. Fig. 10b illustrates results exclusively for catalysts with approximately the same Co surface area (and particle size), as determined from H_2 chemisorption. As illustrated, modifications with Mg have a strong negative impact on FT C_{5+} yield, which is not related to Co particle size, again strongly suggesting a chemical/site-poisoning effect perhaps

comparable to the effect of other alkalies [91]. The effect of Mg is relatively much stronger when co-impregnated with Co–Re than when added to the support prior to high-temperature calcination (1173 K) and then impregnated with Co–Re. The effect of Zn is less clear, since here the particle sizes increased when Zn was co-impregnated with Co–Re. When Zn is added to the support and high-temperature calcined (1173 K) prior to impregnating with Co–Re, C_{5+} yield is actually slightly increased with 5 wt% Zn, even though the C_{5+} selectivity is slightly lower than for the reference catalyst on γ-Al_2O_3 (No. 2).

3.7. Effects from co-feeding water

In a typical gas-to-liquid plant, oxygen-containing species (i.e., water or O_2) are first introduced to the value chain by the production of synthesis gas. In the cobalt-based Fischer–Tropsch synthesis, this oxygen is primarily rejected as water. Thus, the reaction conditions approaching the fixed-bed reactor exit will be increasingly influenced by water and hydrocarbon products. The only alternatives to water formation are the rejection of oxygen as CO_2 or oxygenates, neither of which are desirable for the purpose of hydrocarbon synthesis. The effects of water on Co catalysts were recently reviewed by Dalai and Davis [97].

The purpose of this investigation was to study the effect of water, focusing on catalysts (No. 5 and 6) supported on the mechanically promising material $NiAl_2O_4$-α-Al_2O_3. Previous investigations have shown increased C_{5+} selectivity when water is added during FTS over Co and CoRe catalysts [42], but the effect appears to depend strongly on the support material [42,94,98]. In Fig. 11a, the rate of hydrocarbon production (r_{HC}) is illustrated as a function of time on stream (TOS). This figure can be compared directly to the previous publication of results for SiO_2, TiO_2, and γ-Al_2O_3-supported catalysts [94,99]. The experiments consisted of seven different periods each lasting 20–25 h; A: initial dry conditions, B: adjusted gas feed to reach 50% CO conversion, C: co-feeding He (5 bar), D: co-feeding H_2O (4 bar), E: co-feeding H_2O (6.9 bar), F: co-feeding He (10 bar), and G: same feed as in period B. As previously seen for 12 wt% Co (+0.5 wt% Re) supported on SiO_2 and TiO_2 [94,99], co-feeding water increased hydrocarbon production rates. Removal of diffusion limitations as an explanation for increased rates can be ruled out knowing that removing transport limitations on CO would decrease the rate because of the negative reaction order of CO [6,16]. Deactivation mechanisms in cobalt-based Fischer–Tropsch synthesis was recently reviewed by Tsakoumis et al. [100]. However, extrapolating deactivation rates from period B, there was no sign that co-feeding water had caused any (irreversible) deactivation to these catalysts.

Co-feeding water changes the partial pressures of H_2 and CO, when keeping the synthesis gas feed constant in periods B–G. Co-feeding an inert gas (He) during periods C and E made it possible to obtain partial pressures of water lower than in period B. Fig. 11b and c illustrate the selectivity to C_{5+} and CH_4, respectively, as a function of the average partial pressure of H_2O (the average of inlet and outlet). Using the corresponding average partial pressures of H_2 and CO, the calculated H_2/CO ratios remained fairly constant (1.90–1.94) through periods B–G, which was expected.

It has previously been suggested by Bertole et al. [101] that water increases the amount of active surface carbon, mostly present as monomeric species, while the surface concentration of CO was found to be almost insensitive to the reaction conditions [14]. This observation is supported by a study from Krishnamoorthy et al. [102], where no variation in the intensity or vibrational frequency for CO was observed when co-feeding water. The increased amount of active monomeric carbon species may be caused by an interaction between co-adsorbed water and CO, lowering the barrier to CO activation [101]. Fig. 11d illustrates that hydrogenation of propene is inhibited by higher partial pressures of H_2O, as previously also demonstrated by Aaserud et al. [96]. This inhibition of secondary hydrogenation is most likely caused by a higher total surface concentration of reactants, products, and intermediates, thus leaving fewer sites available for re-adsorption. *In situ* studies will be necessary to confirm or dispute this.

4. Conclusions

Different cobalt catalysts were prepared by incipient wetness impregnation of supports modified by Mg, Zn, or Ni. Two supports modified with 5 wt% Ni and 10 wt% Mg, respectively, were calcined at high temperatures (>1400 K) yielding low surface area alumina with Ni- and Mg-spinel inclusions. These supports exhibited substantially improved mechanical strength compared to α-Al_2O_3 prepared from the same γ-Al_2O_3.

Catalyst dispersion was limited to <10–11%, which is common for samples based on nitrate precursors that are dried and calcined in air. The effect of 0.5 wt% Re on the dispersion and reducibility of cobalt oxide was in accordance with previous publications, promoting the reduction from CoO to Co^0, but without significantly affecting the reduction from Co_3O_4 to CoO. O_2 titration likely underestimated the degree of reduction, which prior to reaction (*ex situ*) most likely was in the range of 85–100%, when including results for all catalysts together.

The effect of Re on Co-based Fischer–Tropsch synthesis studied at 483 K, 20 bar, and H_2/CO = 2 was in accordance with previously published results. Co-impregnating Co–Re with Mg or Zn had a strong negative effect on activity and C_{5+} selectivity. Adding the modification to the support and calcining at a high temperature (1173 K) prior to impregnating with Co–Re, for Mg, the effect was still negative with respect to activity and C_{5+} selectivity, while Zn had no negative effect on C_{5+} yield. Similar effects were seen with respect to increased CO_2 selectivity for all modifications of Mg and Zn, except when Zn was added to the support and calcined at a high temperature (1173 K) before impregnating with Co–Re. Cobalt catalysts are known to have very low water–gas-shift activity. Mg and Zn were estimated to have modified this activity by up to 30%. No amount of Mg or Zn was beneficial for decreasing the amount of CO_2 produced when also considering the negative effects on overall activity and selectivity. In general, the negative effects of Mg and Zn could not be explained by dispersion or particle size effects and were likely related to a chemical/site effect similar to that of alkalies reported on in the literature.

The effect of water for the high-temperature calcined Ni-modified support was in accordance with the literature, improving reaction rates and C_{5+} selectivity, while inhibiting olefin hydrogenation, as demonstrated by the propene/propane ratio.

Acknowledgements

The Norwegian Academy of Science and Letters (VISTA), Statoil and the Department of Chemical Engineering at the Norwegian University of Science and Technology are gratefully acknowledged for financial support. Support materials were provided by Statoil.

References

[1] W. Ngantsoue-Hoc, Y. Zhang, R.J. O'Brien, M. Luo, B.H. Davis, Appl. Catal. A 236 (2002) 77.
[2] J.P. den Breejen, P.B. Radstake, G.L. Bezemer, J.H. Bitter, V. Frøseth, A. Holmen, K.P. de Jong, J. Am. Chem. Soc. 131 (2009) 7197.
[3] P.B. Radstake, J.P. den Breejen, G.L. Bezemer, J.H. Bitter, K.P. de Jong, V. Frøseth, A. Holmen, Stud. Surf. Sci. Catal. 167 (2007) 85.
[4] G.L. Bezemer, J.H. Bitter, H.P.C.E. Kuipers, H. Oosterbeek, J.E. Holewijn, X.D. Xu, F. Kapteijn, A.J. van Dillen, K.P. de Jong, J. Am. Chem. Soc. 128 (2006) 3956.
[5] J.L. Zhang, J.A. Chen, J. Ren, Y.W. Li, Y.H. Sun, Fuel 82 (2003) 581.
[6] R. Zennaro, M. Tagliabue, C.H. Bartholomew, Catal. Today 58 (2000) 309.

[7] E. Iglesia, Appl. Catal. A 161 (1997) 59.
[8] B.G. Johnson, C.H. Bartholomew, D.W. Goodman, J. Catal. 128 (1991) 231.
[9] S.W. Ho, M. Houalla, D.M. Hercules, J. Phys. Chem. 94 (1990) 6396.
[10] J.J.C. Geerlings, M.C. Zonnevylle, C.P.M. de Groot, Surf. Sci. 241 (1991) 315.
[11] J.J.C. Geerlings, M.C. Zonnevylle, C.P.M. de Groot, Surf. Sci. 241 (1991) 302.
[12] D. Schanke, S. Vada, E.A. Blekkan, A.M. Hilmen, A. Hoff, A. Holmen, J. Catal. 156 (1995) 85.
[13] V. Frøseth, S. Storsæter, Ø. Borg, E.A. Blekkan, M. Rønning, A. Holmen, Appl. Catal. A 289 (2005) 10.
[14] C.J. Bertole, G. Kiss, C.A. Mims, J. Catal. 223 (2004) 309.
[15] E. Iglesia, S.L. Soled, R.A. Fiato, J. Catal. 137 (1992) 212.
[16] G.P. Van der Laan, A.A.C.M. Beenackers, Catal. Rev. – Sci. Eng. 41 (1999) 255.
[17] L. Fu, C.H. Bartholomew, J. Catal. 92 (1985) 376.
[18] S. Bessell, Appl. Catal. A 96 (1993) 253.
[19] G. Jacobs, T.K. Das, Y.Q. Zhang, J.L. Li, G. Racoillet, B.H. Davis, Appl. Catal. A 233 (2002) 263.
[20] A.Y. Khodakov, Catal. Today 144 (2009) 251.
[21] Ø. Borg, S. Eri, E.A. Blekkan, S. Storsæter, H. Wigum, E. Rytter, A. Holmen, J. Catal. 248 (2007) 89.
[22] S. Storsæter, B. Tøtdal, J.C. Walmsley, B.S. Tanem, A. Holmen, J. Catal. 236 (2005) 139.
[23] D.Y. Xu, W.Z. Li, H.M. Duan, Q.J. Ge, H.Y. Xu, Catal. Lett. 102 (2005) 229.
[24] T.K. Das, G. Jacobs, P.M. Patterson, W.A. Conner, J.L. Li, B.H. Davis, Fuel 82 (2003) 805.
[25] F. Diehl, A.Y. Khodakov, Oil Gas Sci. Technol.-Rev. Inst. Franc. Petr. 64 (2009) 11.
[26] E. van Steen, M. Claeys, Chem. Eng. Technol. 31 (2008) 655.
[27] E. Iglesia, S.C. Reyes, R.J. Madon, S.L. Soled, Adv. Catal. 39 (1993) 221.
[28] M.E. Dry, Appl. Catal. A 138 (1996) 319.
[29] B.H. Davis, Fuel Process. Technol. 71 (2001) 157.
[30] G. Jacobs, Y. Ji, B.H. Davis, D. Cronauer, A.J. Kropf, C.L. Marshall, Appl. Catal. A 333 (2007) 177.
[31] D.I. Enache, M. Roy-Auberger, R. Revel, Appl. Catal. A 268 (2004) 51.
[32] R. Riva, H. Miessner, R. Vitali, G. del Piero, Appl. Catal. A 196 (2000) 111.
[33] Y. Zhang, H. Xiong, K. Liew, J. Li, J. Mol. Catal. A 237 (2005) 172.
[34] Ø. Borg, S. Storsæter, S. Eri, H. Wigum, E. Rytter, A. Holmen, Catal. Lett. 107 (2006) 95.
[35] A.Y. Khodakov, A. Griboval-Constant, R. Bechara, V.L. Zholobenko, J. Catal. 206 (2002) 230.
[36] D. Song, J. Li, J. Mol. Catal. A 247 (2006) 206.
[37] K. Okabe, K. Murata, M. Nurunnabi, Y.Y. Liu, J. Jpn. Pet. Inst. 52 (2009) 139.
[38] Ø. Borg, N. Hammer, S. Eri, O.A. Lindvåg, R. Myrstad, E.A. Blekkan, M. Rønning, E. Rytter, A. Holmen, Catal. Today 142 (2009) 70.
[39] S. Prachayawarakorn, R. Mann, Catal. Today 128 (2007) 88.
[40] R. Guettel, T. Turek, Chem. Eng. Sci. 64 (2009) 955.
[41] Ø. Borg, P.D.C. Dietzel, A.I. Spjelkavik, E.Z. Tveten, J.C. Walmsley, S. Diplas, S. Eri, A. Holmen, E. Rytter, J. Catal. 259 (2008) 161.
[42] D. Schanke, S. Eri, E. Rytter, C. Aaserud, A.M. Hilmen, O.A. Lindvåg, E. Bergene, A. Holmen, Stud. Surf. Sci. Catal. 147 (2004) 301.
[43] A. Guerrero-Ruiz, A. Sepúlveda-Escribano, I. Rodríguez-Ramos, Appl. Catal. A 120 (1994) 71.
[44] N.N. Madikizela-Mnqanqeni, N.J. Coville, Appl. Catal. A 272 (2004) 339.
[45] N.N. Madikizela-Mnqanqeni, N.J. Coville, Appl. Catal. A 317 (2007) 195.
[46] N.N. Madikizela-Mnqanqeni, N.J. Coville, Appl. Catal. A 340 (2008) 7.
[47] N.N. Madikizela, N.J. Coville, J. Mol. Catal. A 181 (2002) 129.
[48] N.N. Madikizela-Mnqanqeni, N.J. Coville, J. Mol. Catal. A 225 (2005) 137.
[49] X. Long, Z.T. Liu, Z.W. Liu, X.H. Li, K. Fujimoto, Catal. Lett. 131 (2009) 388.
[50] E. Rytter, T.H. Skagseth, S. Eri, A.O. Sjåstad, Ind. Eng. Chem. Res. 49 (2010) 4140.
[51] E. Rytter, T.H. Skagseth, H. Wigum, S. Nonyameko, Fischer-Tropsch catalysts, US Patent, US2007161714 A1.
[52] B.C. Enger, R. Lødeng, J. Walmsley, A. Holmen, Appl. Catal. A 383 (2010) 119.
[53] S. Brunauer, P.H. Emmett, E. Teller, J. Am. Chem. Soc. 60 (1938) 309.
[54] E.P. Barrett, L.G. Joyner, P.P. Halenda, J. Am. Chem. Soc. 73 (1951) 373.
[55] B.H. Isaacs, E.E. Petersen, J. Catal. 85 (1984) 1.
[56] R.C. Reuel, C.H. Bartholomew, J. Catal. 85 (1984) 63.
[57] J. Xiong, Ø. Borg, E.A. Blekkan, A. Holmen, Catal. Commun. 9 (2008) 2327.
[58] E.A. Blekkan, A. Holmen, S. Vada, Acta Chem. Scand. 47 (1993) 275.
[59] J.M. Thomas, W.J. Thomas, Principles and Practice of Heterogeneous Catalysis, VCH Verlagsgesellschaft mbH, Weinheim, 1997.
[60] H.P. Klug, L.E. Alexander, X-ray Diffraction Procedures for Polycrystalline and Amorphous Materials, John Wiley & Sons, New York, 1954.
[61] J.L. Lemaitre, P.G. Menon, F. Delannay, Characterization of heterogeneous catalysts, Chemical Industries Series, vol. 15, Marcel Dekker Inc., New York, 1984.
[62] ASTM, D5757 – Standard Test Method for Determination of Attrition and Abrasion of Powdered Catalysts by Air Jets, doi:10.1520/D5757-00R06.
[63] A.M. Hilmen, E. Bergene, O.A. Lindvåg, D. Schanke, S. Eri, A. Holmen, Catal. Today 105 (2005) 357.
[64] A. Boumaza, L. Favaro, J. Lédion, G. Sattonnay, J.B. Brubach, P. Berthet, A.M. Huntz, P. Roy, R. Tétot, J. Solid State Chem. 182 (2009) 1171.
[65] F.S. Pettit, E.H. Randklev, E.J. Felten, J. Am. Ceram. Soc. 49 (1966) 199.
[66] O. Varnier, N. Hovnanian, A. Larbot, P. Bergez, L. Cot, J. Charpin, Mater. Res. Bull. 29 (1994) 479.
[67] V. Montouillout, D. Massiot, A. Douy, J.P. Coutures, J. Am. Ceram. Soc. 82 (1999) 3299.
[68] R.K. Pati, P. Pramanik, J. Am. Ceram. Soc. 83 (2000) 1822.
[69] M.S. Wang, M. Muhammed, Synthesis and characterisation of $MgAl_2O_4$ spinel ceramic precursor, in: Synthesis and Properties of Mechanically Alloyed and Nanocrystalline Materials, Pts 1 and 2 – Ismanam-96, 1997.
[70] J.J. Guo, H. Lou, H. Zhao, X.G. Wang, X.M. Zheng, Mater. Lett. 58 (2004) 1920.
[71] D.R. Kaar, H.G. Sowman, Microcrystalline transition metal oxide spinel articles, US Patent 4757036.
[72] I. Arslan, J.C. Walmsley, E. Rytter, E. Bergene, P.A. Midgley, J. Am. Chem. Soc. 130 (2008) 5716.
[73] C.K. Rofer-DePoorter, Chem. Rev. 81 (1981) 447.
[74] W.C. Conner, J.L. Falconer, Chem. Rev. 95 (1995) 759.
[75] C.M. Lok, Stud. Surf. Sci. Catal. 147 (2004) 283.
[76] C.M. Lok, Catalysts with high cobalt surface area, US Patent US6927190 B2.
[77] C.M. Lok, S. Bailey, G. Gray, Method for the production of cobalt catalysts supported on silicon dioxide and their use, US Patent US6534436 B2.
[78] M. Wolters, H. Daly, A. Goguet, F.C. Meunier, C. Hardacre, J.H. Bitter, P.E. de Jongh, K.P. de Jong, J. Phys. Chem. C 114 (2010) 7839.
[79] M. Wolters, P. Munnik, J.H. Bitter, P.E. de Jongh, K.P. de Jong, J. Phys. Chem. C 115 (2011) 3332.
[80] M. Wolters, L.J.W. van Grotel, T.M. Eggenhuisen, J.R.A. Sietsma, K.P. de Jong, P.E. de Jongh, Catal. Today 163 (2011) 27.
[81] S. Rane, Ø. Borg, J. Yang, E. Rytter, A. Holmen, Appl. Catal. A 388 (2010) 160.
[82] Ø. Borg, M. Rønning, S. Storsæter, W. van Beek, A. Holmen, Stud. Surf. Sci. Catal. 163 (2007) 255.
[83] A.Y. Khodakov, J. Lynch, D. Bazin, B. Rebours, N. Zanier, B. Moisson, P. Chaumette, J. Catal. 168 (1997) 16.
[84] A.M. Hilmen, D. Schanke, A. Holmen, Catal. Lett. 38 (1996) 143.
[85] V. Bakken, E. Bergene, E. Rytter, O. Swang, Catal. Lett. 135 (2010) 21.
[86] P. Arnoldy, J.A. Moulijn, J. Catal. 93 (1985) 38.
[87] V. Jayaram, B. Sirisha Rani, Mater. Sci. Eng. A 304–306 (2001) 800.
[88] F. Pepe, M. Schiavello, G. Ferraris, J. Solid State Chem. 12 (1975) 63.
[89] A. Navrotsky, A. Muan, J. Inorg. Nuclear Chem. 33 (1971) 35.
[90] Ø. Borg, J.C. Walmsley, R. Dehghan, B.S. Tanem, E.A. Blekkan, S. Eri, E. Rytter, A. Holmen, Catal. Lett. 126 (2008) 224.
[91] C.M. Balonek, A.H. Lillebø, S. Rane, E. Rytter, L.D. Schmidt, A. Holmen, Catal. Lett. 138 (2010) 8.
[92] M. Ojeda, R. Nabar, A.U. Nilekar, A. Ishikawa, M. Mavrikakis, E. Iglesia, J. Catal. 272 (2010) 287.
[93] S. Storsæter, D. Chen, A. Holmen, Surf. Sci. 600 (2006) 2051.
[94] S. Storsæter, Ø. Borg, E.A. Blekkan, B. Tøtdal, A. Holmen, Catal. Today 100 (2005) 343.
[95] E. Rytter, S. Eri, T.H. Skagseth, D. Schanke, E. Bergene, R. Myrstad, A. Lindvåg, Ind. Eng. Chem. Res. 46 (2007) 9032.
[96] C. Aaserud, A.M. Hilmen, E. Bergene, S. Eric, D. Schanke, A. Holmen, Catal. Lett. 94 (2004) 171.
[97] A.K. Dalai, B.H. Davis, Appl. Catal. A 348 (2008) 1.
[98] S. Lögdberg, M. Boutonnet, J.C. Walmsley, S. Järås, A. Holmen, E.A. Blekkan, Appl. Catal. A 393 (2011) 109.
[99] S. Storsæter, Ø. Borg, E.A. Blekkan, A. Holmen, J. Catal. 231 (2005) 405.
[100] N.E. Tsakoumis, M. Rønning, Ø. Borg, E. Rytter, A. Holmen, Catal. Today 154 (2010) 162.
[101] C.J. Bertole, C.A. Mims, G. Kiss, J. Catal. 210 (2002) 84.
[102] S. Krishnamoorthy, M. Tu, M.P. Ojeda, D. Pinna, E. Iglesia, J. Catal. 211 (2002) 422.